



Hydrochemistry and weathering at Pardo River basin, São Paulo State, Brazil

Daniel Marcos Bonotto

Received: 23 June 2022 / Accepted: 27 February 2023 / Published online: 3 April 2023
© The Author(s), under exclusive licence to Springer Nature Switzerland AG 2023

Abstract This work was conducted at the Pardo River hydrographic basin, which is a federal watershed belonging to the Paranapanema River hydrographic basin (PRHB) in Brazil (São Paulo State and Paraná State). The aim was to realize an integrated hydrochemical and radiometric (U-isotopes and ^{210}Po) approach, highlighting the water/soil-rock and surface water/groundwater interactions, with implications to the weathering processes occurring there. The study area has been often considered one of the best preserved/unpolluted river in São Paulo State, contributing to the water supply of several cities distributed along its banks. However, the results reported here suggest possible lead diffuse pollution caused by the use of phosphate fertilizers in agricultural activities taking place in the basin. The analyzed groundwaters and surface waters tend to be neutral to slightly alkaline (pH of 6.8–7.7), possessing low mineral concentration (total dissolved solids up to 500 mg/L). SiO_2 is the major dissolved constituent in the waters, while bicarbonate is the dominant anion, and calcium is the preponderant cation. The effects of the weathering of silicates to control the dissolution of constituents in the liquid phase have been identified from some diagrams often utilized in hydrogeochemical

studies. Chemical weathering rates have been estimated from hydrochemical data associated to analytical results of the natural uranium isotopes ^{238}U and ^{234}U concerning to samples of rainwater and Pardo River waters. The fluxes in this watershed are permitted to obtain the following rates: 11.43 t/km² year (sodium), 2.76 t/km² year (calcium), 3.17 t/km² year (magnesium), 0.77 t/km² year (iron), and 8.64 t/km² year (uranium). This new dataset constitutes valuable information for people engaged on the management of the Pardo River watershed, as well as to researchers interested on comparative studies considering the available data from other basins worldwide.

Keywords Hydrochemistry · Surface waters · Groundwaters · Pardo River watershed · Chemical weathering rates

Introduction

The lithosphere-pedosphere-hydrosphere interaction establishes the boundary condition for life on Earth. This is because water and nutrients extracted from rocks and soils are essential for all forms of life. EarthLabs (2022) pointed out that such interaction also affects the fate and transport of pollutants, implying the cycling of fluids and metals in the Earth's crust, storage of hydrocarbons in sedimentary basins, modeling and evolution of the landscape, and evolution of geothermal and volcanic activities. On

D. M. Bonotto (✉)
São Paulo State University-UNESP, Av. 24-A No. 1515,
P.O. Box 178, CEP 13506-900 Rio Claro, São Paulo,
Brazil
e-mail: danielmarcosbonotto@gmail.com

long timescales, it affects the distribution of CO₂ in the atmosphere and climate evolution. The water circulating in a hydrographic basin brings information about the geogenic and anthropic relationships, since the use and occupation of land in a basin influence the quality of its natural resources, modifying them (Anjinho et al., 2020). Thus, the conservation of the quantity and quality of water depends on the natural and human conditions of the hydrographic basins, from where it originates, circulates, percolates, or is stored, whether in the form of natural lakes or artificial reservoirs (Capobianco & Whately, 2002; Ouma et al., 2022).

Several techniques have contributed in recent decades to the improvement of knowledge about water/soil-rock interactions and, consequently, weathering processes, including natural radionuclides in this context. Bonotto (2022a) reported some studies that are also relevant for the purpose of this paper: Moreira-Nordemann (1980, 1984), Pačes (1983), Baskaran (1995), White and Blum (1995), Schulz and White (1999), Small et al. (1999), Jeter (2000), Grasby and Hutcheon (2000), Chabaux et al. (2001, 2003), Millot et al. (2002), Duan et al. (2002), Riebe et al. (2003), Krishnaswami et al. (2004), Dosseto et al. (2008), and Dellinger et al. (2017). Weathering is an important phenomenon of the geochemical cycle, since it contributes to the formation of relief, comprising, in a general way, the physical and chemical changes undergone by rocks due to their exposure to different conditions of humidity and temperature (Bertin, 1974). Weathering is also considered as the process by which a rock disintegrates or decomposes, a phenomenon that occurs on the Earth's surface and whose main cause is the interaction of the rock itself with water (Netto, 1980). By mechanical weathering (disintegration), rocks are gradually fragmented into smaller pieces, while by chemical weathering (decomposition), the production of new substances/compounds occurs due to reactions (oxidation, hydration, carbonation, dissolution, etc.) between the constituents of the atmosphere and the rocks (Bertin, 1974).

In general, weathering processes are slow, being the type and duration controlled by the climate; however, different lithotypes are also expected to imply different weathering rates (Pačes, 1983). Once weathered and disaggregated, the source rock provides fragments that can give rise to soils or constitute sediments, that is, deposits of solid material formed by a

mobile medium (wind, ice, or water) on the Earth's surface (Laporte, 1969).

The hydrographic basin constitutes the ideal unit for researches focusing weathering processes, because, in it, physical and chemical processes take place that shape the relief and condition the relationships between its biotic and abiotic components (Piroli, 2013). Water forms the link between these components, because, when it precipitates over this space, it is directed to regions determined by its cycle, forming streams and rivers that run on the surface or infiltrate into sub-surface reservoirs, feeding aquifers or springs that will maintain the water courses in the periods between precipitations (Piroli, 2013).

In Brazil, according to Law No. 9,433 (Brasil, 1997), the hydrographic basin is the basic unit for the management of water resources, being defined as an area with physical and biological characteristics delimited by its water dividers, in which the human being lives and interacts, and where surface and groundwater are displaced, under the action of gravity, to a stream, river, or reservoir (surface or underground), by channels that converge into a larger watercourse that can flow into a main river, natural/artificial water reservoir, swamp, or directly in an ocean (Piroli, 2013).

Thus, a watershed comprises the entire area of natural rainwater catchment that provides surface runoff to the main channel and its tributaries, with the watershed (topographic divide) being its upper limit, and its outlet (confluence) the lower limit (Lima, 2006). Therefore, the watershed constitutes the surface area that drains water, sediments, and dissolved materials to a common outlet, at a given point in a river channel, varying in size and articulating from main drainage dividers (Coelho Netto, 2005). Rodrigues and Adami (2005) consider the watershed as a system close to the Earth's surface, carrying mostly solid and liquid materials, which is internally and externally delimited by all the processes that, from the supply of water by the atmosphere, interfere with the flow of matter and energy in a river or a network of river channels. Dibieso (2007) recognizes that water is the most important natural resource in a hydrographic basin, suggesting that its quality is closely related to the uses and activities carried out in the basin. Leal (1995) also points out the direct or indirect repercussion on the rivers and on the quality and quantity of the water of what happens in the hydrographic

basin; that is, what happens to the elements, materials, and energies present in the area will affect all of themselves.

In summary, the water circulating in a hydrographic basin brings information about the geogenic and anthropic relationships, since the use and occupation of land in a basin influence the quality of its natural resources, modifying them. The preservation or removal of riparian forests on the banks of rivers impacts the ecosystem of the basin, as they act as physical barriers to the processes of transporting materials to the waters, maintaining the stability of the banks of springs and rivers (Piroli, 2013). In the same way that rivers and streams feed a dam, for example, they can also bring debris and polluting materials that may be dumped directly on them or on the soils through which their waters passed (Capobianco & Whately, 2002).

Two different Pardo River watersheds occur at São Paulo State, Brazil, where the name “Pardo” refers to the predominant color (brownish) of their waters, especially in the rainy season, due to the red latosols predominant in those areas (Cavalchuki, 2021). The first basin is located in the northeast region of the state and belongs to the Grande River hydrographic basin (GRHB) which is a federal basin that contains areas at São Paulo State and Minas Gerais State. The second basin is located in the center/southwest region of São Paulo State, which is part of the Paranapanema River hydrographic basin (PRHB), being also a federal basin as it contains areas in the States of São Paulo and Paraná.

This paper will focus this last Pardo River watershed that is considered one of the best preserved/unpolluted river in São Paulo State, whose waters are classified as class 2, implying on possible use for domestic supply, after conventional treatment; the protection of aquatic communities; primary contact recreation (water skiing, swimming, and diving); and the natural and/or intensive pisciculture (Cavalchuki, 2021). It is one of the largest rivers in the south of São Paulo State, supplying several cities distributed along its banks, even generating energy with some plants installed in its bed.

The Pardo River of this study is a source of development in the various sectors of the economy of its basin, contributing to the water supply of about 5 million inhabitants (population density of ~50 inhabitants per km²) unevenly distributed along the PRHB.

Thus, the importance of this watershed coupled to the rainfall and discharge data series available since the 1950s justify the integrated hydrochemical and radiometric (U-isotopes and ²¹⁰Po) approach realized here. We highlight the water/soil-rock and surface water/groundwater interactions, with implications to the weathering processes occurring at the Pardo River basin, aiming to generate helpful information for people engaged on its management, as well to researchers interested on comparative studies considering the available data from other basins worldwide.

Major features of the study area

The Pardo River watershed of this study is located in the northern portion of the PRHB and east of the Paraná Sedimentary Basin (PSB), between the parallels 22°15' and 23°15' of south latitude and the meridians 48°15' and 50°00' of west longitude (Fig. 1). In this watershed, the Pardo River is 264 km long within São Paulo State, from its source in Limoeiro Mountain Range, near the urban domain of the municipality of Pardinho, at 982 m of altitude, to its mouth, at the Lucas Nogueira Garcez dam in the city of Salto Grande (São Paulo State), at an altitude of 377 m, where it is an important tributary on the right side of the Paranapanema River (CBH-MP, 1999). On its route, it travels through fifteen cities, being the main river of the Middle PRHB (UGRHI-17) (Fig. 1), which is made up of 42 cities.

The drainage area of the studied Pardo River watershed is approximately 4800 km², with about 3281 springs that originate 437 tributaries of first to fourth order. The headwater regions are generally characterized with higher drainage density (Piroli, 2013). According to Safre and Manzione (2015), the main tributaries of the Pardo River are as follows: Claro River, which rises in the municipality of Botucatu, has its confluence with the Pardo River in the municipality of Iaras, having a length of 72 km; Novo River, which rises in the municipality of Itatinga, has its confluence in the Pardo River in the municipality of Águas de Santa Bárbara, having 77 km in length; Turvo River, which is the main tributary of the Pardo River, rises in the municipality of Agudos, has its confluence in the Pardo River in the municipality of Ourinhos and is 130 km long.

(a)



(b)



◀**Fig. 1** **a** Location of São Paulo State in Brazil. **b** Location of the Pardo River watershed at São Paulo State and sampling points in this study. 1, Ourinhos (ORN); 2, Santa Cruz do Rio Pardo (SCP); 3, Águas de Santa Bárbara (ASB); 4, Avaré (AVR); 5, Botucatu (BOT); 6, Pardo (PRN)

Geologically, the study area is located at the PSB that constitutes a large intracratonic basin (synclisis) on the South American platform, which comprises the south and southeast of Brazil and other South American countries (Milani et al., 2007). The PSB covers a vast area of 1,700,000 km² with an elongated shape in the NE-SW direction. It has a package of sedimentary and magmatic rocks that reaches about 7000 m at its depocenter, which is located in the state of Paraná, just below the homonymous river (Morelato, 2017). The PSB is composed of six supersequences of sedimentation and subsidence separated by erosive intervals, related to the interaction of tectonic and eustatic events from the beginning of the Ordovician to the end of the Cretaceous (Milani & Ramos, 1998). The supersequences occurring in the study area are Gondwana III and Bauru.

The Gondwana III supersequence comprises the stratigraphic interval of the PSB in which the Botucatu and Serra Geral Formations (the São Bento Group) are

located (Silva et al., 2003). The Botucatu Formation consists mainly of medium to fine pinkish sandstones of high sphericity, with tangential cross bedding of medium to large size, characteristically of aeolian origin (Milani et al., 2007). The Serra Geral Formation, in turn, is the result of an intense fissure magmatism, dated around 132 Ma, characterized by a thick cover of flows, about 1500 m thick at the depocenter of the basin, associated with a wide network of dikes and numerous sills intruded into the sedimentary layers. In the study area, the Serra Geral Formation (JKsg) (Fig. 2) occurs along the main rivers and to the west, near the mouth of the Pardo River, presenting volcanic tholeiitic rocks, in basaltic flows of gray to black color, texture aphanitic, with intercalations of intertrap sandstones from the Botucatu Formation (IPT, 1981, Perrotta et al., 2005).

The Bauru supersequence is neocretaceous, corresponding to a post-basaltic cover of psammitic siliciclastic character generated under semi-arid to desert conditions (Milani et al., 2007). It consists of Caiuá and Bauru Groups with gradual and interdigitated lateral passage (Fernandes, 2004), being relevant for the study area the Bauru Group and its formations Adamantina (Ka) and Marília (Km) (Fig. 2). The Adamantina

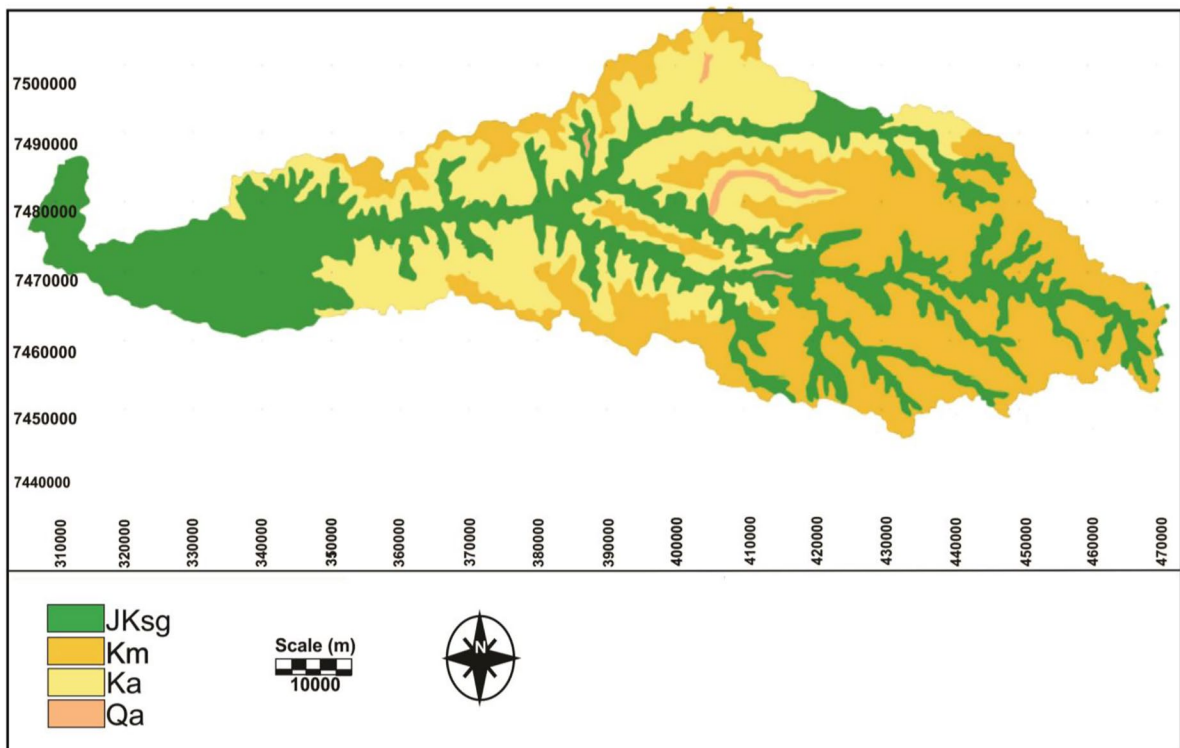


Fig. 2 Simplified geological map of Pardo River watershed. According to Piroli (2013)

Formation is composed of tabular metric layers of sandstones, intercalated with siltstones or sandy mudstones. The sandstones found can be fine to very fine, light brown to orange in color, of moderate to good selection, being massive or with small to medium-sized tabular to channel cross-bedding, and occasionally intense carbonate cementation. The silty strata that occur interspersed are cream to brown in color, with a massive structure or unremarkable plane-parallel bedding and contraction cracks and bioturbation features in the upper portions (Fernandes, 2004). The Marília Formation (Fig. 2) is generally characterized by massive sandstones and subordinate conglomerates, both with carbonate cementation (Albarelli, 2013). Among its subdivisions, Echaporã Member is relevant for the study area, consisting of fine to medium sandstones, with intense carbonate cementation, immature, with coarse fractions, and infrequent granules; subordinately, carbonate crusts, sandy mudstones, and conglomeratic (centimetric) lithofacies also occur (Milani et al., 2007).

In addition to the aforementioned formations, in the study area, there are also some insignificant patches of Quaternary deposits (Qa) (Fig. 2) associated with alluvium from the rivers of the studied hydrographic basin, which are defined by deposits on the banks, channel bottoms, and plains of river flooding, which may be dominated by sand, gravel, silt, clay, and, locally, peat resulting from erosive processes, followed by transport and deposition of varied source areas (Perrotta et al., 2005).

The Pardo River watershed is geomorphologically inserted into the unit defined as São Paulo State Western Plateau, under the morphostructural unit of the PSB, a domain that occupies approximately 50% of the total state area. The plateau basement consists chiefly on the rocks of the Bauru Group, mostly sandstones, while rocks of the Serra Geral Formation are found in the valleys formed where the Paranapanema and Pardo Rivers flow (Ross & Moroz, 1997, CBH-MP, 1999). Regarding the relief, the study area is characterized by basaltic *cuestas* in the region of the main sources of the Pardo, Claro, and Novo rivers. Thus, the main sources of Pardo River are in the Botucatu Residual Plateau, where the dominant occurrences are hills with broad tops, whose altitudes vary between 600 and 900 m, with dominant slopes between 10 and 20% (Piroli, 2013). The central region and the mouth of the Pardo River basin are within the Central Western Plateau where the reliefs are slightly undulating with a predominance of broad and low

hills with flat tops and altitudes varying between 300 and 600 m, with the dominant slopes between 10 and 20% (Ross & Moroz, 1997).

The predominant soils in the Pardo River basin are the red latosols, distributed over most of its area, and the nitisols located to the Southeast, in small patches in the higher altitude regions and in a larger patch in the central-west region of the basin (Piroli, 2013). In addition to these, there are also two patches of red-yellow latosol in the area, located in the sub-basins of the Novo River (to the Southeast) and the Claro River (to the Northeast), and four patches of argisols, located to the east, north, and center-west of the Pardo basin. (Oliveira et al., 1999). The main use of the basin's soil is for agricultural purposes. Pasture areas are dominant throughout the basin area, followed by areas of temporary cultivation of sugarcane, soybean, corn, and pine, mainly in the western portion, and then by forestry areas, concentrated in the east of the study area. Less expressively, portions of permanent coffee and orange cultivation are found in the central and eastern regions, patches of sparse remaining forests, and urban patches associated with the main municipalities in the region (CBH-RP, 2016).

According to the IBGE (2002), the climate of the region is classified as Tropical Central Brazil, sub-hot (with average temperatures between 15 and 18 °C in at least 1 month), and humid. To the south of the Plateau, on the banks of the Paranapanema River, zones of tropical climate appear, with hot summers, without a dry season in winter, of the Cfa type (Piroli, 2013). The moist season occurs between December and March (summer) while the dry period between July and August (winter). Figure 3 shows the monthly rainfall and flow rate data as measured from 1955 to 2020 at the Pardo River watershed. August and January are the driest and wettest

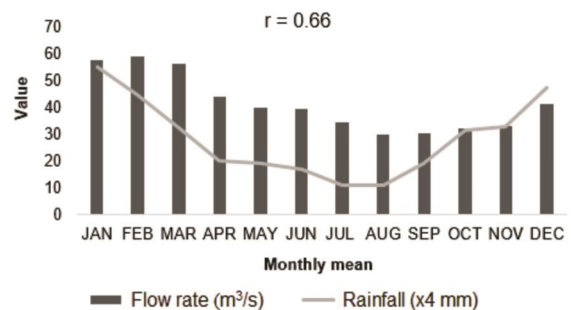


Fig. 3 Monthly rainfall and flow rate measured, respectively, at the monitoring stations D6-006 and 6D-002 (Águas de Santa Bárbara spa), in the period 1955–2020. Data reported by DAEE (2021)

months, in which the mean precipitation corresponded to 43.2 and 220.5 mm, respectively (Fig. 3). Figure 3 has been plotted from data reported by DAEE (2021) in the period 1955–2020 at the monitoring stations D6-006 and 6D-002 for rainfall and discharge, respectively, that are located at Águas de Santa Bárbara spa. Figure 3 indicates that the flow rate at Pardo River and rainfall correlate significantly as the Pearson’s correlation coefficient is $r=0.66$ (the p value is 0.0195).

The two geological units that dominate the study area (Bauru and Serra Geral) also form the two main aquifers. The Bauru aquifer occurs with less expressiveness only in the north of the area, being characterized as continuous, of regional extension, being free or confined, and of moderate to low transmissivity. The Serra Geral aquifer, on the other hand, is discontinuous and also of regional extension, however, with porosity and permeability associated with fractures, columnar disjunctions, and vesicles (CBH-MP, 2019). In the study area, waters from the Guarani Aquifer System (GAS) and other aquifers are exploited by deep tubular wells. Silva (1983), Sracek and Hirata (2002), Bonotto (2006), and Cresswell and Bonotto (2008), among others, have investigated the GAS considering tubular wells drilled along transects established at São Paulo State. The geological substrate of the GAS is associated with the sandstones of the Botucatu and Pirambóia Formations, whose outcrops were initially described in the municipalities of Botucatu and Pirambóia (currently Anhembi), constituting recharge areas for the GAS and located in the UGRHI-10 (Sorocaba/Médio Tietê), which interfaces with the UGRHI-17.

Sampling and analytical methods

Six monitoring points at Pardo River have been selected for collecting surface water samples at the following sites (Fig. 1): 1, Ourinhos (ORN); 2, Santa Cruz do Rio Pardo (SCP); 3, Águas de Santa Bárbara (ASB); 4, Avaré (AVR); 5, Botucatu (BOT); 6, Pardinho (PRN). Groundwater samples have also been taken at a 120-m depth tubular well that was drilled at the left margin of Pardo River at Águas de Santa Bárbara spa, which exploits the Serra Geral and GAS aquifers as shown in the profile plotted in Fig. 4. The sampling campaigns were conducted between September 2017 and November 2018. Also relevant

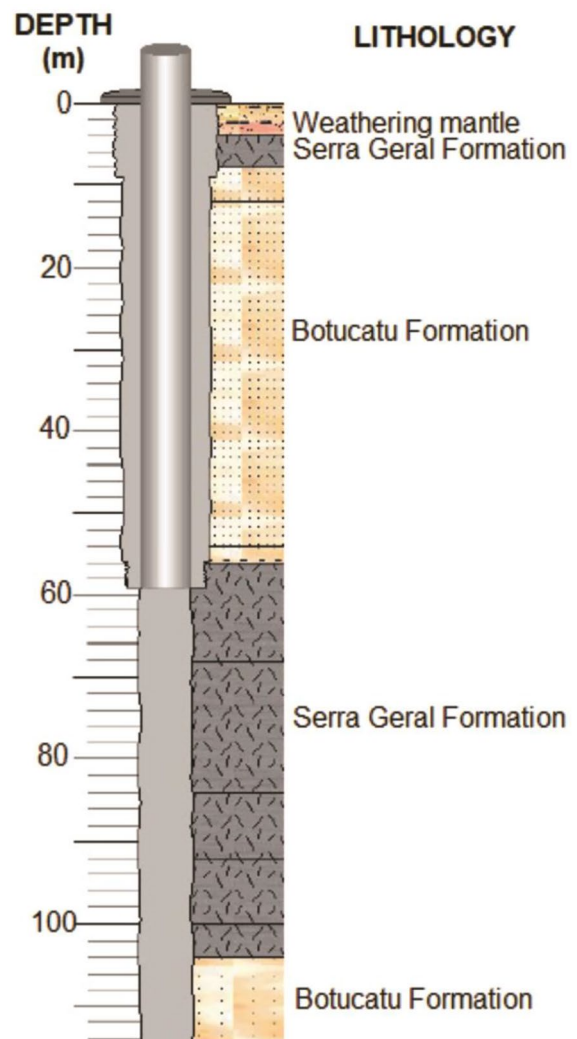


Fig. 4 Description of the tubular well drilled at Águas de Santa Bárbara spa that exploits waters from GAS and Serra Geral aquifers. According to SIAGAS (2022)

for this study are the rainwater data reported by Soler i Gil and Bonotto (2015) in two stations of the Pardo River watershed.

The containers for sampling corresponded to bottles of polyethylene possessing volume between 2 and 20 L. Before collecting the samples, HNO₃ (10%) was used for their initial washing, followed by rinsing with purified water (Milli-Q) and afterwards a final cleaning with the own waters to be collected. The physicochemical data were measured in the field whereas the chemical parameters in the laboratory, adopting the steps and methods already reported by Bonotto

and Thomazini (2019). Temperature, pH, electrical conductivity (EC), and potential redox (Eh) measurements were done in situ by potentiometry (Bonotto, 2006). The alkalinity data for each water sample were acquired by titration with 0.02 N H_2SO_4 (100 mL aliquot) (Hach, 2000).

The bottles containing the water samples were taken to LABIDRO-Isotopes and Hydrochemistry Laboratory and LARIN-Ionizing Radiations Laboratory of IGCE/UNESP/Rio Claro-SP, Brazil. Millipore membranes (0.45 μm) were used for filtering the water samples, which were after preserved with HCl or HNO_3 and separated into different aliquots for obtaining the hydrochemical composition of major and trace elements/compounds, including radionuclides (^{238}U , ^{234}U , and ^{210}Po). The following methods were adopted for the data acquisition: (1) atomic absorption spectrometry (AAS), Ca^{2+} ; (2) flame photometry, Na^+ and K^+ ; (3) colorimetry, SiO_2 , Mg^{2+} , Cl^- , NO_3^- , NO_2^- , NH_4^+ , SO_4^{2-} , and PO_4^{3-} (DL between 6 $\mu\text{g/L}$ and 0.8 mg/L, depending on the parameter); (4) potentiometry with ion selective electrode (ISE), F^- ; (5) total reflection X-ray fluorescence spectroscopy (TXRF), Fe, Mn, Cr, Sr, Ba, Cu, Zn, Pb, and Ni. The detection limit of these techniques has been reported by Bonotto (2022b); for instance, it ranged from 6 to 0.8 mg/L for colorimetry (Bonotto, 2022b). The sum of the concentration of main dissolved cations, anions, and silica in the analyzed waters allowed to estimate the total dissolved solids (TDS). Hach (2000), van de Wiel (2003), Bonotto and Silveira (2003), and Bonotto and Roveratti (2017) have provided additional information about these analytical procedures.

The dissolved ^{210}Po in the waters was recovered from a volume of circa 10 L from each sample. A known amount (0.2 mL; activity = 40 dpm/mL) of ^{209}Po spike was added to assess ^{210}Po recovery. Hydroxylamine hydrochloride (20%, 5 mL) plus sodium citrate solution (25%, 2 mL) were added into a Teflon beaker (50 mL capacity) containing each sample. Then, ammonia was used to adjust the pH to 2 as described by Flynn (1968). Thereafter, the solution was put in a magnetic stirrer with a hot plate, and a 2.5-cm diameter copper disc was immersed in it for plating the polonium. The heating temperature was 85–90 °C and the stirring time corresponded to 75–90 min by means of a Teflon stirrer. After the disc removal, it was rinsed (with demineralized H_2O) and a heating lamp was used for drying it. Finally, the planchet was inserted in a vacuum chamber

for conventional alpha counting. The spectroscopic system utilized a EG&G ORTEC Model BU-020–450-AS ULTRA-AS Ion-Implanted Detector with B-Mount possessing the following characteristics: 0.1-mm depletion depth, 450 mm^2 active area, and alpha resolution of 20 keV FWHM at 5.486 MeV. The alpha spectra containing the peaks associated to the polonium isotopes (^{209}Po and ^{210}Po) were recorded by the EG&G ORTEC 919 Spectrum Master Multichannel Buffer (1024 channels) that was coupled to the detector and controlled by the MAESTRO simulator software. The calibration of the system was realized by the use of a standardized radioactive source (^{232}U – ^{228}Th). The energy region varied between 4.8 and 5.5 MeV. The ^{210}Po activity concentration in the water samples was determined adopting the isotope dilution principle (Bonotto, 2010).

The ^{238}U activity concentration and $^{234}\text{U}/^{238}\text{U}$ activity ratio (AR) data were obtained after extracting the uranium isotopes ^{238}U and ^{234}U from another water aliquot of approximately 20 L. It was acidified to $\text{pH} < 2$ (with HCl), and ~500 mg of FeCl_3 plus ^{232}U spike (4.4 dpm) were added. Next, the steps described by Bonotto (2017) were adopted as follows. U was co-precipitated on $\text{Fe}(\text{OH})_3$ by increasing the pH to 7–8 through addition of concentrated NH_4OH solution; the precipitate was recovered, dissolved in 8 M HCl, and Fe^{3+} was extracted into an equal volume of isopropyl ether. The acid U-bearing solution was purified by a strong chloride anion exchanger, first on a Cl^- and then on a NO_3^- column of 100–200 mesh Dowex 1-X8 resin. U was finally eluted from the NO_3^- column with 0.1 M HCl and, after evaporation to dryness, was dissolved in 10 mL of 2 M $(\text{NH}_4)_2\text{SO}_4$ electrolyte and transferred to an electrodeposition cell. The pH was adjusted to 2.4, and electrodeposition of U on a stainless steel planchet was completed after 3 h at a current density of 1 Acm^{-2} . The ^{238}U activity concentration and AR were measured by alpha spectrometry as described for ^{210}Po and also based on the isotope dilution principle but in this case considering the counting rate measured in the peaks of ^{238}U , ^{234}U and ^{232}U . In the literature, there are additional descriptions for these measurements, for instance, Bonotto et al. (2009) and Bonotto (2010), among others. The statistical uncertainties of the readings at 1 σ standard deviation and 5% significance level (Young, 1962) were generally between 10 and 15%.

Rock samples from Bauru and Serra Geral Formations were chemically analyzed by high-end wavelength

dispersion XRF (X-ray fluorescence) performed with a Philips PW 2400 spectrometer as described by Bonotto and Roveratti (2020). The ^{238}U activity concentration and AR data were obtained by alpha spectrometry adopting radiochemical procedures similar to those used for the water samples. However, in this case, the rock samples (0.5–3.0 g) were initially digested with 1:3 $\text{HNO}_3\text{-HCl}$ (*aqua regia*). The analytical results obtained in this study are reported in Tables 1, 2, and 3.

Discussion

Water quality and use in agriculture

For drinking water, WHO (2011) proposed limiting values for the ingestion of several dissolved constituents due to their health constraints. Among the analyses realized in this paper, the limits and restrictions are for the following parameters: 0.7 mg/L for Ba; 50 mg/L for nitrate (as NO_3^-); 1.5 mg/L for fluoride; 50 $\mu\text{g/L}$ for Cr; 10 $\mu\text{g/L}$ for Pb; and 30 $\mu\text{g/L}$ for ^{238}U . Additionally, taste (not health) thresholds for Cl^- of 200–300 mg/L were also suggested, depending on the associated cation (WHO, 2011). The dataset reported in Tables 1 and 2 indicate that Pb is the unique chemical analyzed that exceeded the guidance level (10 $\mu\text{g/L}$) in some surface and groundwater samples. The potential source of its presence in the Pardo River waters is the diffuse pollution caused by the use of phosphate fertilizers in agricultural activities taking place in the basin, as such fertilizers used to be an entrance way for soil contamination with heavy metals, chiefly cadmium and lead (Freitas et al., 2009).

Human beings can suffer health threats when ingesting water containing dissolved natural radionuclides above certain activity concentration levels. Birke et al. (2010) pointed out that agricultural activities, among others, may be responsible by the inputs of uranium (^{238}U) and some of its decay products (for instance, ^{226}Ra , ^{210}Pb , etc.) in the watercourses. Bonotto (2022b) claimed that generally concentration values between 0.1 and 10 $\mu\text{g/L}$ for dissolved uranium have been reported in different water bodies such as rivers, lakes, and groundwaters as also previously outlined by Fritz and Fontes (1980) and Ivanovich and Harmon (1992). WHO (2011) proposed maximum levels of 30 $\mu\text{g/L}$ and 10 Bq/L, respectively, for the ^{238}U concentration

and ^{238}U activity concentration in potable waters. Such limits are, respectively, 1000 and ~28,000 times higher than the biggest values given in Table 2 (0.03 $\mu\text{g/L}$, equivalent to 0.36 mBq/L).

The WHO (2011) guidance levels for ingesting these radionuclides in waters are 1 Bq/L (for ^{234}U) and 0.1 Bq/L (for ^{210}Po). Table 2 shows that the biggest activity concentration values corresponded to 1.24 mBq/L (for ^{234}U , as calculated from the ^{238}U activity concentration and $^{234}\text{U}/^{238}\text{U}$ activity ratio) and 45.6 mBq/L (for ^{210}Po) that not surpassed the WHO (2011) limiting values.

USSL (1954) grouped 16 types of waters in a chart, according to the values of EC and sodium adsorption ratio (SAR). The diagram has been applicable to define the water usefulness for the purposes of irrigation and growing plants in agricultural soils (Mirabbasi et al., 2008; Wilcox, 1955). Figure 5 shows a SAR vs. EC diagram containing the rainwater, groundwaters, and surface waters data given in Table 1. All these waters are inserted in the C1-S1 field, alike most of those analyzed by Bonotto (2022b), who suggested that they are low saline and sodic waters, with possible use for irrigating most of the soil types.

Major hydrochemical features

The mean pH of 6.4 in rainwater (Table 1) indicates a slightly acid precipitation in the study area, similarly to findings in other areas, for instance, Araxá City at Minas Gerais State, Brazil (Bonotto, 2022b). The analyzed groundwaters and surface waters tend to be neutral to slightly alkaline (mean pH values between 6.8 and 7.7) (Table 1). The parameters pH and Eh reflect, respectively, the protons and electrons activities in the environment. In natural environments, oxidizing acid and reducing basic systems are often reported in the literature, with the pH and Eh correlating inversely (Baas Becking et al., 1960; Brownlow, 1996; Krauskopf & Bird, 1995). Such tendency has been also confirmed in the groundwaters exploiting the GAS and Serra Geral aquifers as shown in Fig. 6 ($r=0.67$, p value = 0.0087).

Usually, surface waters tend to reach TDS values lower than those of groundwaters as confirmed by the data of this study (Table 1; mean value in the groundwater samples = 154 mg/L; range of the values obtained for surface waters = 39–74 mg/L). They possess very low mineral concentration (TDS < 50 mg/L) and low

Table 1 Physicochemical and major dissolved constituents data of the water samples analyzed in this study. Rainwater data reported by Soler i Gil and Bonotto (2015). All sampling sites are located at São Paulo State

Sam- pling site— remark	Latitude	Longitude	Sampling date	Code	Temp. (°C)	pH	Eh (mV)	EC (µS/ cm)	^b TDS (mg/L)	SiO ₂ (mg/L)	HCO ₃ ⁻ (mg/L)	CO ₃ ²⁻ (mg/L)	Cl ⁻ (mg/L)	SO ₄ ²⁻ (mg/L)	NO ₃ ⁻ (mg/L)	Na ⁺ (mg/L)	K ⁺ (mg/L)	Ca ²⁺ (mg/L)	Mg ²⁺ (mg/L)
Rainwater																			
^c BOT	22°58'30"S	48°29'30"W	-	RW1	nm	6.2	nm	100	8	2.6	3	0	1.76	0.27	1.96	0.21	0.25	0.42	0.08
^d ASB	22°52'50"S	49°14'15"W	-	RW2	nm	6.6	nm	110	12	2.0	6	0	0.97	1.00	1.51	0.56	0.49	1.07	0.18
Mean			-	RW	nc	6.4	nc	105	10	2.3	4.5	0	1.36	0.64	1.74	0.38	0.37	0.74	0.13
Groundwaters																			
^d ASB	22°52'50"S	49°14'15"W	09/13/2017	GW1	31.7	8.0	235	196	140	14.3	90	0	0.20	<1	0.2	15.9	2.03	15.44	0.73
^d ASB	22°52'50"S	49°14'15"W	11/16/2017	GW2	30.1	8.0	234	169	160	26.8	94	0	0.30	1	0.5	13.6	1.68	20.86	0.62
^d ASB	22°52'50"S	49°14'15"W	12/08/2017	GW3	28.0	7.4	267	169	135	10.1	94	0	0.30	<1	0.3	13.1	1.68	14.64	0.70
^d ASB	22°52'50"S	49°14'15"W	01/08/2018	GW4	29.1	7.9	226	169	141	10.1	94	0	0.20	1	0.2	13.8	1.72	18.68	0.60
^d ASB	22°52'50"S	49°14'15"W	02/17/2018	GW5	33.0	6.8	259	171	166	33.5	92	0	0.50	1	0.3	15.9	1.68	20.34	0.68
^d ASB	22°52'50"S	49°14'15"W	03/15/2018	GW6	30.4	7.9	244	172	165	33.6	92	0	0.30	<1	0.3	16.8	1.60	19.68	0.69
^d ASB	22°52'50"S	49°14'15"W	04/19/2018	GW7	28.5	7.8	212	165	162	33.2	94	0	0.60	1	1.6	14.7	1.91	13.46	0.71
^d ASB	22°52'50"S	49°14'15"W	05/16/2018	GW8	28.8	7.8	217	167	165	33.7	92	0	1.60	<1	0.2	15.6	2.61	18.42	0.67
^d ASB	22°52'50"S	49°14'15"W	06/21/2018	GW9	33.2	6.4	284	182	153	32.4	82	0	0.80	<1	0.6	16.8	2.11	17.05	0.65
^d ASB	22°52'50"S	49°14'15"W	07/12/2018	GW10	32.0	6.4	256	176	148	27.7	80	0	0.40	1	0.6	16.1	1.99	17.25	0.67
^d ASB	22°52'50"S	49°14'15"W	08/10/2018	GW11	29.5	6.2	287	176	152	32.4	80	0	0.70	<1	0.6	16.3	2.11	16.86	0.38
^d ASB	22°52'50"S	49°14'15"W	09/14/2018	GW12	30.7	7.4	290	187	157	31.2	82	0	2.90	1	0.7	15.0	3.82	18.13	0.43
^d ASB	22°52'50"S	49°14'15"W	10/10/2018	GW13	28.5	7.0	305	168	158	32.9	84	0	3.60	1	0.6	14.0	2.15	18.87	0.79
^d ASB	22°52'50"S	49°14'15"W	11/12/2018	GW14	29.7	7.0	295	164	157	32.1	84	0	2.10	<1	0.6	15.0	2.46	17.52	0.74
^d ASB - mean	22°52'50"S	49°14'15"W	-	GW	30.2	7.3	258	174	154	27.4	88	0	1.04	1	0.5	15.2	2.11	17.66	0.65
Surface waters																			
^c ORN	22°56'30"S	49°54'43"W	11/16/2017	RP1a	nm	7.2	287	169	62	14.3	32	0	2.0	<1	0.9	3.9	1.21	5.96	0.87
^c ORN	22°56'30"S	49°54'43"W	09/14/2018	RP1b	nm	7.6	284	65	58	15.6	24	0	3.9	1	0.6	3.2	1.56	6.04	1.66
^c ORN	22°56'30"S	49°54'43"W	10/10/2018	RP1c	nm	6.2	304	52	51	13.1	18	0	4.4	2	1.4	2.5	1.87	4.56	0.87
^c ORN	22°56'30"S	49°54'43"W	11/12/2018	RP1d	nm	7.2	304	74	58	17.1	20	0	4.8	1	1.8	3.2	1.17	6.54	0.91
^c ORN - mean	22°56'30"S	49°54'43"W	-	RP1	nc	7.0	295	90	57	15.0	23.5	0	3.8	1	1.2	3.2	1.45	5.78	1.08
^f SCP	22°54'16"S	49°37'10"W	11/16/2017	RP2	nm	7.2	294	64	59	14.3	28	0	1.7	1	1.3	3.9	0.86	5.26	2.00
^d ASB	22°52'50"S	49°14'15"W	10/10/2017	RP3a	nm	7.6	177	56	48	12.0	22	0	1.9	1	0.6	3.0	1.09	5.56	0.56
^d ASB	22°52'50"S	49°14'15"W	11/16/2017	RP3b	nm	7.2	299	52	59	25.9	20	0	1.8	1	0.4	2.8	0.86	4.62	1.75
^d ASB	22°52'50"S	49°14'15"W	12/08/2017	RP3c	nm	7.3	304	50	46	11.1	22	0	2.1	1	0.4	2.5	0.78	5.01	0.49
^d ASB	22°52'50"S	49°14'15"W	01/08/2018	RP3d	nm	7.6	287	45	35	3.8	20	0	1.4	1	0.3	2.3	0.86	4.41	0.90

Table 1 (continued)

Sam- pling site— remark	Latitude	Longitude	Sampling date	Code	Temp. (°C)	pH	Eh (mV)	^a EC (µS/ cm)	^b TDS (mg/L)	SiO ₂ (mg/L)	HCO ₃ ⁻ (mg/L)	CO ₃ ²⁻ (mg/L)	Cl ⁻ (mg/L)	SO ₄ ²⁻ (mg/L)	NO ₃ ⁻ (mg/L)	Na ⁺ (mg/L)	K ⁺ (mg/L)	Ca ²⁺ (mg/L)	Mg ²⁺ (mg/L)
^d ASB	22°52'50"S	49°14'15"W	02/17/2018	RP3e	nm	7.8	225	52	54	3.6	20	0	1.9	1	0.4	3.7	0.59	21.54	0.72
^d ASB	22°52'50"S	49°14'15"W	03/15/2018	RP3f	nm	7.5	246	55	95	14.3	54	0	1.6	1	0.5	5.1	0.59	16.80	0.71
^d ASB	22°52'50"S	49°14'15"W	04/19/2018	RP3g	nm	7.3	275	49	50	12.9	22	0	1.7	1	0.4	5.3	0.51	4.67	1.00
^d ASB	22°52'50"S	49°14'15"W	05/16/2018	RP3h	nm	7.4	234	51	61	9.5	22	0	2.7	1	0.6	3.5	1.44	18.54	1.00
^d ASB	22°52'50"S	49°14'15"W	06/21/2018	RP3i	nm	6.7	273	54	46	13.8	18	0	2.1	<1	1.0	4.1	0.86	4.74	0.82
^d ASB	22°52'50"S	49°14'15"W	07/12/2018	RP3j	nm	6.6	303	59	47	14.0	18	0	2.3	<1	1.3	3.9	1.13	4.97	0.86
^d ASB	22°52'50"S	49°14'15"W	08/10/2018	RP3k	nm	6.4	275	47	40	9.6	16	0	2.3	<1	0.7	3.5	1.56	4.27	1.40
^d ASB	22°52'50"S	49°14'15"W	09/14/2018	RP3l	nm	8.0	256	60	53	11.2	20	0	8.4	1	0.8	4.4	1.21	5.20	0.34
^d ASB	22°52'50"S	49°14'15"W	10/10/2018	RP3m	nm	7.0	281	40	42	10.8	14	0	5.2	<1	1.0	2.1	1.76	3.98	1.36
^d ASB	22°52'50"S	49°14'15"W	11/12/2018	RP3n	nm	7.4	274	55	52	14.0	20	0	3.0	<1	1.0	3.7	0.98	5.25	1.90
^d ASB - mean	22°52'50"S	49°14'15"W	-	RP3	nc	7.3	265	52	52	11.9	22	0	2.7	1	0.7	3.6	1.02	7.82	0.99
^e AVR	22°57'27"S	48°48'16"W	11/16/2017	RP4	nm	7.2	294	62	74	25.1	30	0	1.0	1	3.2	3.0	0.78	4.94	1.45
^f BOT	22°58'30"S	48°29'30"W	11/17/2017	RP5	nm	7.7	288	33	39	16.8	14	0	1.3	1	0.3	2.3	0.66	2.13	0.60
^h PRN	23°45'38"S	48°23'12"W	11/17/2017	RP6	nm	6.8	294	88	69	13.0	28	0	5.6	1	0.9	12.0	1.40	4.97	1.65

nm not measured, nc not calculated

^aEC electrical conductivity

^bTDS total dissolved solids

^cBOT Botucatu

^dASB Águas de Santa Bárbara

^eORN Ourinhos

^fSCP Santa Cruz do Rio Pardo

^gAVR Avaré

^hPRN Pardinho

Table 2 Minor/trace constituents and dissolved radionuclides data in the water samples analyzed in this study. Rainwater data reported by Soler i Gil and Bonotto (2015)

Sampling site—remark	Code	F ⁻ (mg/L)	PO ₄ ³⁻ (mg/L)	Br ⁻ (mg/L)	NO ₂ ⁻ (mg/L)	NH ₄ ⁺ (mg/L)	Fe _{total} (mg/L)	Sr (mg/L)	Ni (mg/L)	Cu (mg/L)	Zn (mg/L)	Mn (mg/L)	Cr (mg/L)	Ba (mg/L)	Pb (mg/L)	²¹⁰ Po (mBq/L)	²³⁸ U (μg/L—mBq/L)	²³⁴ U/ ²³⁸ U ^b AR	²³⁴ U (mBq/L)
Rainwater																			
^a BOT	RW1	nm	<0.10	0.030	0.005	<0.01	0.01	0.004	0.001	0.002	0.004	0.002	0.0007	0.003	0.0009	nm	<0.002—<0.02	nm	nc
^a ASB	RW2	nm	<0.10	0.010	0.005	<0.01	0.01	0.005	0.002	0.004	0.006	0.004	0.0006	0.008	0.0009	nm	<0.002—<0.02	nm	nc
Mean	RW	nc	<0.10	0.020	0.005	<0.01	0.01	0.004	0.002	0.003	0.005	0.003	0.0006	0.006	0.0009	nc	<0.002—<0.02	nm	nc
Groundwaters																			
^a ASB	GW1	0.07	0.40	0.001	0.005	0.02	0.025	0.071	0.001	0.002	0.131	0.001	0.002	<0.001	0.001	0.83	0.03—0.36	3.46	1.24
^a ASB	GW2	0.08	0.16	0.001	0.005	<0.01	0.007	0.068	<0.001	0.004	0.114	<0.001	<0.001	<0.001	0.005	nm	nm	nm	nc
^a ASB	GW3	0.08	0.12	0.002	0.004	<0.01	0.053	0.016	<0.001	0.001	0.004	<0.001	<0.001	<0.001	<0.001	nm	nm	nm	nc
^a ASB	GW4	0.08	0.16	0.001	0.005	0.01	0.040	0.066	<0.001	0.017	0.196	0.001	0.001	<0.001	0.004	nm	nm	nm	nc
^a ASB	GW5	0.07	0.15	<0.001	0.004	<0.01	0.040	0.026	<0.001	0.017	<0.001	<0.001	<0.001	<0.001	0.001	nm	nm	nm	nc
^a ASB	GW6	0.07	0.03	0.001	0.005	<0.01	0.035	0.045	<0.001	0.009	0.094	<0.001	0.016	<0.001	0.005	nm	nm	nm	nc
^a ASB	GW7	0.07	0.16	0.007	0.004	<0.01	0.062	0.132	<0.001	0.009	0.207	<0.001	<0.001	<0.001	0.012	nm	nm	nm	nc
^a ASB	GW8	0.08	0.09	0.005	0.004	<0.01	0.026	0.043	0.001	0.010	0.207	0.002	<0.001	<0.001	0.003	nm	nm	nm	nc
^a ASB	GW9	0.07	0.13	0.004	0.004	0.01	0.074	0.112	<0.001	0.046	0.206	0.009	0.001	<0.001	0.011	nm	nm	nm	nc
^a ASB	GW10	0.07	0.33	0.008	0.005	0.03	0.071	0.033	0.003	0.022	1.311	0.010	<0.001	<0.001	0.002	nm	nm	nm	nc
^a ASB	GW11	0.07	0.12	0.012	0.005	0.12	0.266	0.075	0.005	0.016	2.164	0.018	<0.001	<0.001	0.001	nm	nm	nm	nc
^a ASB	GW12	0.07	0.06	0.003	0.004	<0.01	0.055	0.050	0.003	<0.001	1.778	0.039	<0.001	<0.001	0.003	nm	nm	nm	nc
^a ASB	GW13	0.09	0.04	0.001	0.005	<0.01	0.015	0.062	0.001	0.022	0.028	0.002	0.003	<0.001	0.005	nm	nm	nm	nc
^a ASB	GW14	0.07	0.08	0.006	0.004	0.12	0.827	0.102	0.006	0.096	1.597	0.023	<0.001	<0.001	0.026	nm	nm	nm	nc
^a ASB - mean	GW	0.07	0.14	0.004	0.004	0.02	0.114	0.064	0.003	0.021	0.618	0.012	0.006	<0.001	0.006	nm	nm	nm	nc
Surface waters																			
^c ORN	RP1a	nm	0.17	0.004	0.013	0.04	0.022	0.028	<0.001	0.008	0.015	<0.001	<0.001	0.10	0.010	nm	nm	nm	nc
^c ORN	RP1b	nm	0.04	<0.001	0.005	<0.01	0.003	0.049	0.11	<0.001	0.034	<0.001	<0.001	<0.001	0.004	nm	0.01—0.13	1.85	0.24
^c ORN	RP1c	nm	0.09	0.010	0.006	<0.01	0.013	0.039	0.24	0.002	0.072	<0.001	<0.001	<0.001	0.027	nm	0.01—0.14	3.13	0.43
^c ORN	RP1d	nm	0.07	0.021	0.009	<0.01	0.728	0.067	<0.001	0.024	0.044	0.012	<0.001	<0.001	0.006	nm	0.008—0.10	5.13	0.51
^c ORN - mean	RP1	nc	0.09	0.009	0.008	0.01	0.192	0.046	0.088	0.008	0.040	0.003	<0.001	<0.001	0.012	nc	0.01—0.12	3.37	0.41
^f SCP	RP2	nm	0.15	<0.001	0.005	0.03	0.007	0.068	<0.001	0.004	0.114	<0.001	<0.001	<0.001	0.005	nm	nm	nm	nc

Table 2 (continued)

Sampling site—remark	F ⁻ (mg/L)	PO ₄ ³⁻ (mg/L)	Br ⁻ (mg/L)	NO ₂ ⁻ (mg/L)	NH ₄ ⁺ (mg/L)	Fe _{total} (mg/L)	Sr (mg/L)	Ni (mg/L)	Cu (mg/L)	Zn (mg/L)	Mn (mg/L)	Cr (mg/L)	Ba (mg/L)	Pb (mg/L)	²¹⁰ Po (mBq/L)	²³⁸ U (μg/L—mBq/L)	²³⁴ U/ ²³⁸ U ^b AR	²³⁴ U (mBq/L)
^d ASB RP3a	nm	0.11	0.002	0.005	<0.01	0.044	0.008	<0.001	0.002	0.012	<0.001	<0.001	0.001	<0.001	5.0	nm	nm	nc
^d ASB RP3b	nm	0.06	0.003	0.006	0.01	0.035	0.017	<0.001	0.001	0.012	<0.001	<0.001	0.029	0.003	7.0	nm	nm	nc
^d ASB RP3c	nm	0.19	0.002	0.005	<0.01	0.053	0.016	<0.001	0.001	0.004	<0.001	<0.001	<0.001	<0.001	15.3	nm	nm	nc
^d ASB RP3d	nm	0.15	0.007	0.004	<0.01	0.241	0.022	0.001	0.004	0.016	<0.001	<0.001	<0.001	0.012	5.3	nm	nm	nc
^d ASB RP3e	nm	0.05	0.006	0.004	0.02	0.468	0.036	<0.001	0.004	0.036	0.006	0.001	<0.001	0.019	45.6	nm	nm	nc
^d ASB RP3f	nm	0.03	0.012	0.004	<0.01	0.254	0.333	<0.001	0.008	0.015	0.011	<0.001	<0.001	0.021	4.0	nm	nm	nc
^d ASB RP3g	nm	0.16	0.003	0.004	<0.01	0.490	0.014	0.003	0.019	0.019	<0.001	<0.001	<0.001	0.008	12.6	nm	nm	nc
^d ASB RP3h	nm	0.14	0.007	0.004	<0.01	0.434	0.004	<0.001	0.024	0.043	0.032	<0.001	<0.001	0.003	8.3	nm	nm	nc
^d ASB RP3i	nm	0.25	0.004	0.005	<0.01	0.616	0.023	0.001	0.004	0.013	0.008	<0.001	<0.001	0.004	6.0	nm	nm	nc
^d ASB RP3j	nm	0.19	0.005	0.004	<0.01	0.065	<0.001	<0.001	0.007	0.017	<0.001	<0.001	<0.001	0.002	20.5	nm	nm	nc
^d ASB RP3k	nm	0.05	0.009	0.005	0.18	0.841	<0.001	0.003	0.024	0.066	0.022	0.002	<0.001	0.006	4.7	nm	nm	nc
^d ASB RP3l	nm	0.07	<0.001	0.006	<0.01	0.294	0.008	<0.001	0.008	<0.001	0.003	<0.001	<0.001	0.001	1.4	nm	nm	nc
^d ASB RP3m	nm	0.05	0.014	0.005	<0.01	0.860	0.050	0.003	0.042	0.500	0.011	0.004	<0.001	0.004	2.5	nm	nm	nc
^d ASB RP3n	nm	0.10	0.009	0.005	0.01	1.939	0.054	0.011	0.052	0.092	0.019	<0.001	<0.001	0.005	2.2	nm	nm	nc
^d ASB - RP3 mean	nc	0.11	0.006	0.005	0.02	0.474	0.049	0.004	0.017	0.065	0.014	0.002	0.015	0.007	12.4	nc	nc	nc
^a AVR RP4	nm	0.23	0.002	0.036	<0.01	0.063	0.016	0.001	0.005	0.017	<0.001	<0.001	0.29	0.004	nm	nm	nm	nc
^c BOT RP5	nm	0.03	0.003	0.005	<0.01	0.060	0.018	<0.001	0.036	0.082	<0.001	<0.001	0.12	0.008	nm	nm	nm	nc
^b PRN RP6	nm	0.06	0.007	0.004	<0.01	0.003	0.021	<0.001	0.009	0.014	0.002	<0.001	0.05	0.004	nm	nm	nm	nc

nm not measured, nc not calculated

^aMonitoring point located at São Paulo State

^bAR activity ratio

^cBOT Botucatu

^dASB Águas de Santa Bárbara

^eORN Ourinhos

^fSCP Santa Cruz do Rio Pardo

^gAVR Avaré

^hPRN Pardinho

Table 3 Results of the analysis of dominant rocks occurring in the study area

Parameter	Unit	Sample						Mean
		1	2	3	4	5	6	
Group	-	Bauru	Bauru	Bauru	São Bento	São Bento	São Bento	-
Formation	-	-	-	-	Serra Geral	Serra Geral	Serra Geral	-
Lithology	-	Sandstone	Sandstone	Siltstone	Diabase	Diabase	Basalt	-
SiO ₂	%	87.66	67.59	90.49	49.21	48.19	50.90	65.67
Na ₂ O	%	0.37	1.05	0.28	0.16	0.16	2.57	0.76
K ₂ O	%	1.08	1.99	1.54	0.97	0.80	1.42	1.30
CaO	%	0.08	4.19	0.09	8.49	10.48	8.75	5.35
MgO	%	0.87	1.35	0.33	2.30	4.43	5.25	2.42
Al ₂ O ₃	%	4.13	6.07	4.09	7.03	6.95	12.61	6.81
Fe ₂ O ₃	%	3.14	3.68	1.86	8.31	7.66	14.17	6.47
MnO	%	0.02	0.06	0.03	0.20	0.19	0.20	0.12
TiO ₂	%	0.46	1.13	0.68	4.66	3.82	3.20	2.32
P ₂ O ₅	%	0.02	0.04	0.01	0.37	0.31	0.39	0.19
LOI ^a	%	2.16	12.87	0.61	16.98	16.05	0.54	8.20
U	ppm	0.04	0.12	0.09	3.82	2.87	1.99	1.49
AR ^b	-	1.29	1.25	1.19	1.12	1.10	1.16	1.18

^aLOI loss on ignition

^bAR ²³⁴U/²³⁸U activity ratio

mineral concentration (TDS=50–500 mg/L), based on the TDS classes as reported by van der Aa (2003).

The Piper (1944) and Schoeller (1962) diagrams are useful to plot the obtained hydrochemical data (Table 1). This was done by using the Aquachem 4.0 software (Waterloo Hydrogeologic, 2003) as illustrated in Fig. 7. The SiO₂ concentration is more pronounced in all waters analyzed. Except chloride and nitrate, the remaining constituents are depleted in rainwater as indicated by the Schoeller (1962) diagram (Fig. 7). In terms of dissolved anions, the surface waters and groundwaters are dominated by bicarbonate, while the mixed character is evidenced in the rainwater. The Piper (1944) diagram tends to classify all waters as mixed based on the dissolved cations, but the Schoeller (1962) diagram indicates slight preponderance of calcium in them.

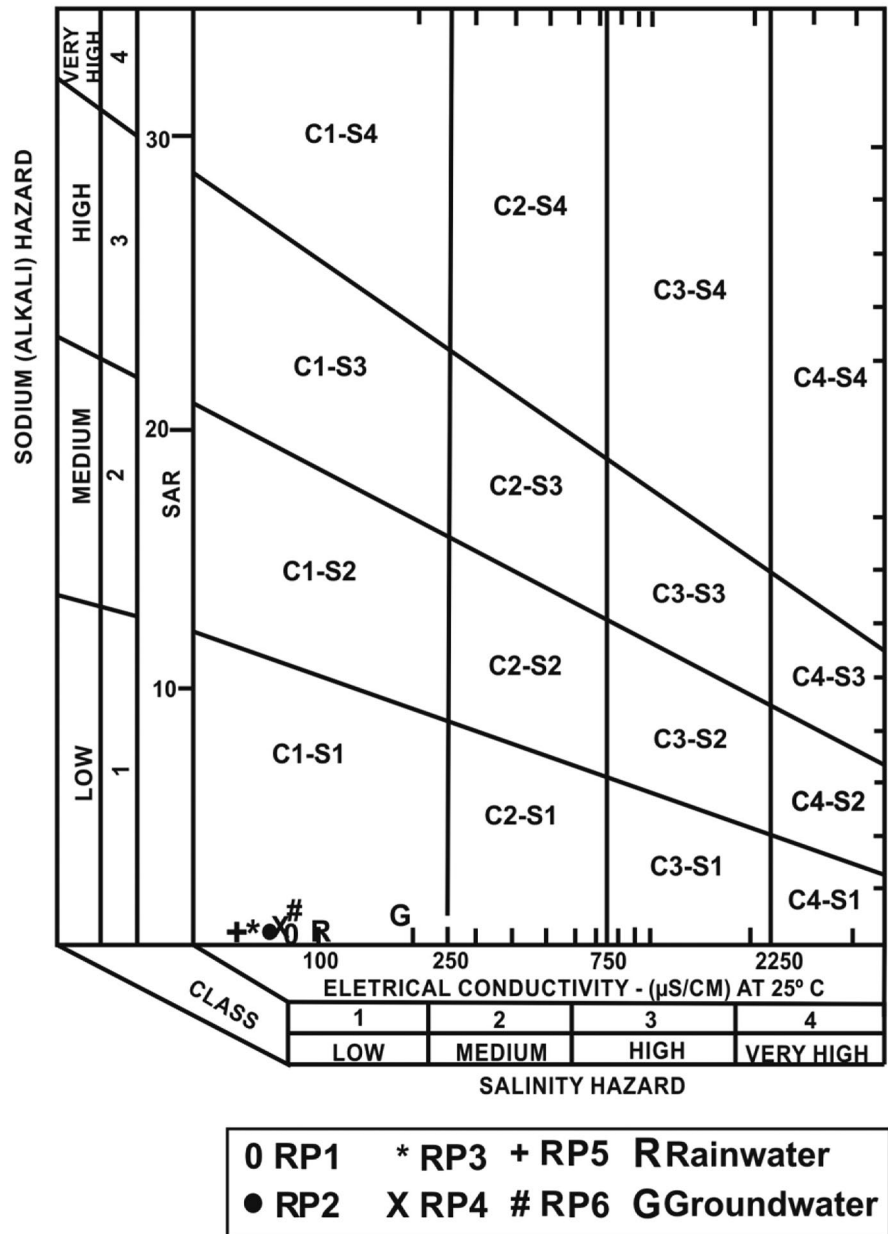
Such hydrochemical facies reflects on some relationships found for the Pardo River waters. The monthly monitoring conducted at Águas de Santa Bárbara spa indicated the following significant correlations (Fig. 8): TDS and Ca ($r=0.62$, p value=0.0205); TDS and bicarbonate ($r=0.90$, p value=0.0001); TDS and Na ($r=0.55$, p value=0.0416). Significant correlation was found between the dissolved Ca and

bicarbonate in the waters of Pardo River collected in 16 and 17 November 2017 at the six monitoring stations (Fig. 8d; $r=0.91$, p value=0.0118).

Direct relationships were determined involving the pairs of parameters pH-bicarbonate ($r=0.79$, p value=0.0008) and TDS-silica ($r=0.89$, p value=0.0001) for the groundwaters exploiting the GAS and Serra Geral aquifers (Fig. 9). The groundwaters composition may be suffering influence of interactions occurring with the surface waters of Pardo River as evidenced by significant correlations involving the following parameters measured during the sampling period of September 2017 to November 2018 (Fig. 9): TDS ($r=0.59$, p value=0.0264); pH ($r=0.64$, p value=0.0137); Na ($r=0.64$, p value=0.0137); Cl ($r=0.84$, p value=0.0002); Fe ($r=0.88$, p value=0.0001). The surface waters-groundwaters interactions could justify some Pb inputs into the aquifer systems, causing their possible Pb contamination as indicated by the measured values in some samples.

The hydrogeochemical data of ocean waters, rainwaters, and surface waters that are compartments of the hydrological cycle have been displayed in boomerang diagrams (Gibbs, 1970) in order to investigate influences and mechanisms affecting them as well as the chemistry of surface waters worldwide. Figure 10

Fig. 5 Use of the USSL (1954) diagram for classifying the salinity hazard of the water samples of this study



shows the analytical data reported in Table 1 as plotted in the Gibbs diagrams; they suggest that the amount of dissolved salts supplied by rainfall as well by the rocks weathering processes chiefly controls the chemical composition of the surface waters and groundwaters.

The lithological influences on the hydrochemistry due to silicates weathering, dissolution of carbonates and evaporates, etc. have been investigated from HCO₃/Na vs. Ca/Na and Mg/Na vs. Ca/Na plots as proposed by Gaillardet et al. (1999) and Kumar (2014).

Figure 11 shows the insertion of the dataset obtained in this study in effects of the weathering of silicates to control the dissolution of constituents in surface waters (Pardo River) and groundwaters (aquifers: GAS + Serra Geral). This is compatible with the more accentuated SiO₂ concentration in typical rock types of the study area (48–90%, Table 3), as well with the high dissolved SiO₂ concentration in these waters (Table 1 and Fig. 7). Thus, the effects of the weathering of silicates to control the dissolution of constituents in the liquid phase

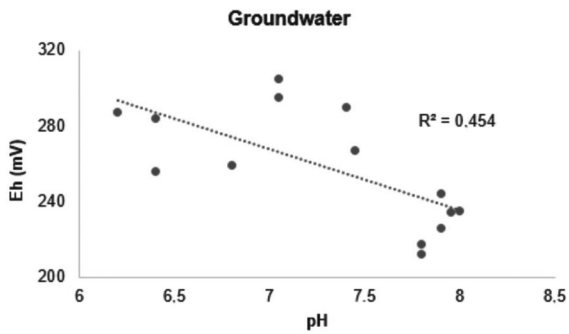


Fig. 6 The Eh–pH relationship in groundwaters sampled at the tubular well shown in Fig. 4

have been identified from some diagrams often utilized in hydrogeochemical studies.

Chemical weathering rates

The concentration of anions, cations, and other constituents in the waters of a watershed, together with the discharge (flow rate) in the watershed and its surface area, allows to calculate the specific transport of the components in the hydrographic basin. Table 4 reports the total flux values calculated at the Pardo River exutory (monitoring point 1, Ourinhos City–ORN) based on the concentration (average) of the constituents obtained for the sampling campaigns realized in September, October, and November 2018 (Tables 1 and 2), the mean flow rate in that period (30 m³/s), and the basin surface area (4803.1 km²).

For a certain dissolved constituent (E), Moreira-Nordemann (1980, 1984) proposed an equation to calculate the parameter W (in t/km² year), representing the amount of weathered matter removed in the hydrographic basin divided by its surface area and time. Bonotto (2022a) used with success a modified expression of this parameter W , taking into account the net flux of the dissolved constituent (F_E , t/km² year) and the constituent concentration in rocks dominantly occurring in the watershed (E_R , dimensionless). It is given by:

$$W = F_E/E_R \quad (1)$$

The net flux may be calculated by subtracting the total flux (transport) of the constituent in the water body of its atmospheric deposition. A negative net

flux value indicates that rainfall deposition surpasses fluvial transport for that constituent, whereas a positive one suggests the opposite. Additional premises and mass balance equations sometimes can be used to realize adjustments for taking into account anthropic inputs and other factors. Examples in the literature are given by Garrels and MacKenzie (1967), White and Blum (1995), Grasby and Hutcheon (2000), and Fernandes et al. (2016), among others.

Table 4 reports the atmospheric deposition (annual value) for the relevant constituents of this study. The following parameters were used on the calculation: average concentration of the constituent in rainwater (values above the detection limit in Tables 1 and 2); average annual precipitation in the period 1955–2021 (1365.35 mm); conversion factor of 1 mm rainfall = 1 L/m². Table 4 shows that the atmospheric inputs were higher than 1 t/km² year following the sequence $\text{HCO}_3^- > \text{SiO}_2 > \text{NO}_3^- > \text{Cl}^- > \text{Ca}^{2+}$.

Table 4 also indicates the following net fluxes above 0: Na⁺, Ca²⁺, Mg²⁺, Fe, Sr, Ni, Zn and Pb. However, among them, there are only rock analysis data available for Na₂O, CaO, MgO, and Fe₂O₃ as reported in Table 3. Therefore, Na, Ca, Mg, and Fe are potentially useful elements for estimating chemical weathering rates based on Eq. (1). The mean concentration of Na₂O, CaO, MgO, and Fe₂O₃ given in Table 3 allows to get the following E_R values: 0.0056 (Na), 0.038 (Ca), 0.0145 (Mg), and 0.0453 (Fe). Thus, adopting such E_R values and considering the corresponding net flux for each element (Table 4), the use of Eq. (1) permits to estimate chemical weathering rates between 0.77 (Fe) and 11.43 t/km² year (Na) as shown in the last column of Table 4.

The U presence in rainwater can be disregarded as its concentration is too low (<0.002 µg/L, Table 2). Table 4 reports a flux value of 1.93×10^{-6} t/km² year as calculated for this radioelement at the Pardo River exutory taking into account the mean dissolved U concentration there (0.01 µg/L, Table 2). Such flux value and $E_R = 1.49 \times 10^{-6}$ for U (Table 3) allow to determine a chemical weathering rate of 1.30 t/km² year according to Eq. (1), which is between 0.77 t/km² year and 2.76 t/km² year as calculated considering the elements Fe and Ca, respectively (Table 4).

Moreira-Nordemann (1980, 1984) defined a solubility coefficient (k , dimensionless) from the analysis of ²³⁸U and its radiogenic product ²³⁴U in rocks, waters, and soils. This factor has been applied in

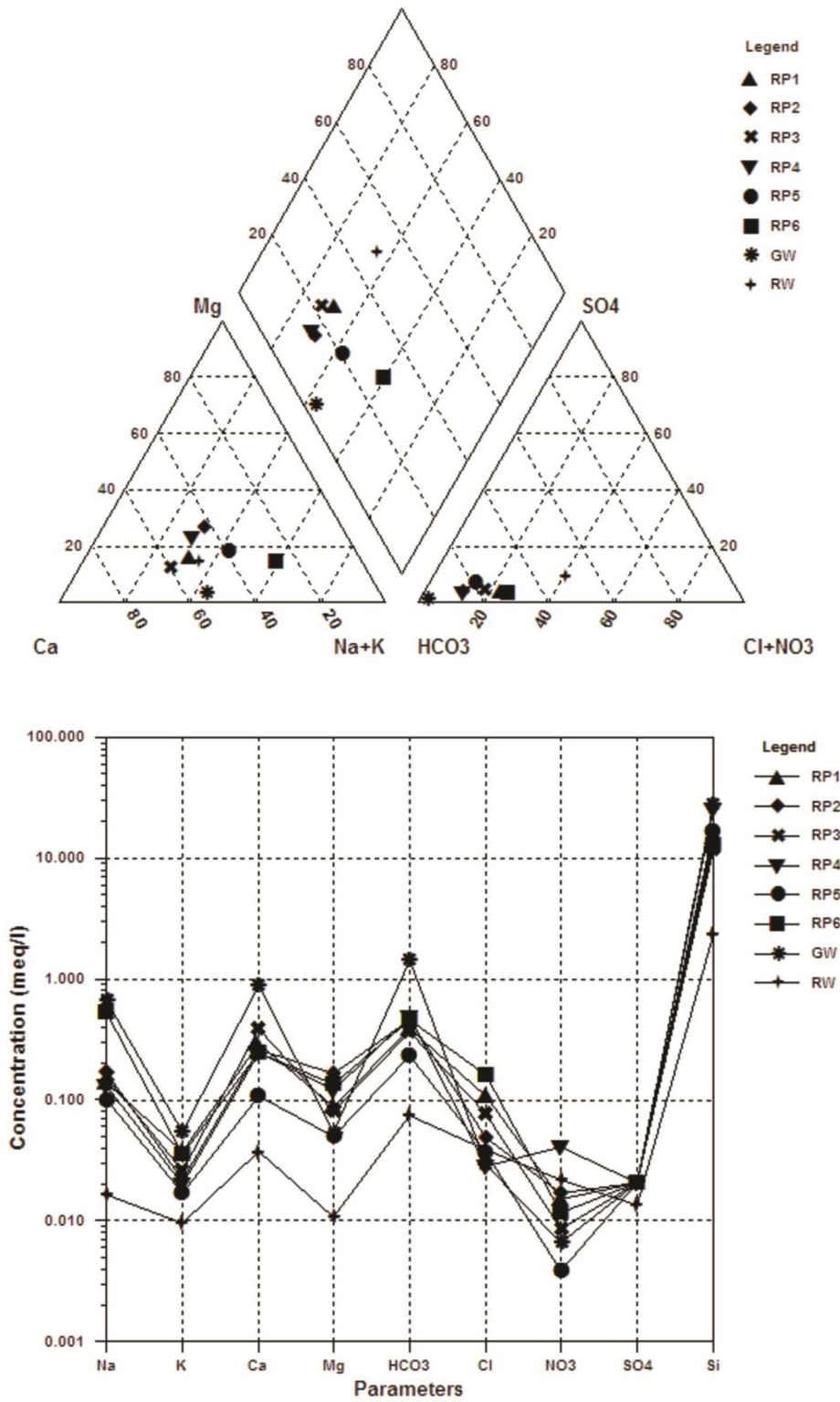


Fig. 7 Use of the Piper (1944) and Schoeller (1962) diagrams for identifying the major hydrochemical facies of the water samples of this study. The codes of the samples are the same of those shown in Table 1

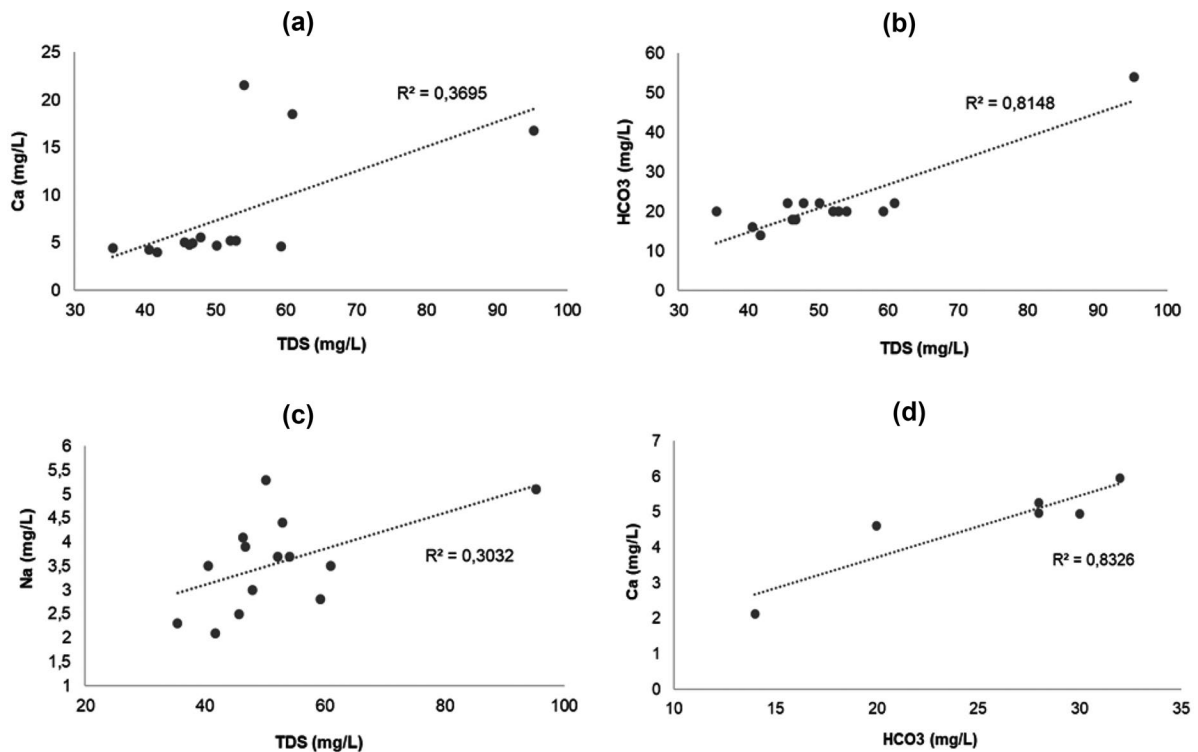


Fig. 8 a–c Relationships found for the Pardo River waters during the monthly monitoring conducted at Águas de Santa Bárbara spa. **d** Relationship between calcium and bicarbonate

at the six monitoring stations for the water samples of Pardo River collected in 16 and 17 November 2017

estimates of chemical weathering rates. The following formula expresses such solubility coefficient for U:

$$k = (A_R - A_S) / (A_L - A_S) \quad (2)$$

where A_R , A_L , and A_S correspond to the $^{234}\text{U}/^{238}\text{U}$ ratio in rocks, waters, and soils, respectively.

Table 3 shows a mean $^{234}\text{U}/^{238}\text{U}$ ratio of 1.18 in typical rocks of the study area, suggesting secular radioactive equilibrium conditions between ^{238}U and ^{234}U ($AR=1$), within experimental errors (10–15%). Ivanovich and Harmon (1992) pointed out that this situation is expected after circa 1 million years for uranium within minerals and rock matrices that remained closed systems for this radioelement.

Dissolved uranium exhibiting values of $AR > 1$ are generally found as a consequence of the rock-water interactions (Baskaran, 2012; Ivanovich & Harmon, 1992; Osmond & Cowart, 1976), which have been also confirmed by data reported in Table 2 (ARs

between 1.85 and 5.13). In this study, it was adopted the A_L value corresponding to 3.37 in Eq. (2) that is the mean AR at the Pardo River exutory (Table 2).

AR values in horizons of different soil profiles at the PSB have been reported by Bonotto et al. (2017), and a representative value of latosols occurring in the study area is $A_S = 0.80 \pm 0.06$ for the Cr horizon from a soil profile sampled close to Piracicaba City, São Paulo State.

Therefore, the insertion of $A_R = 1.18$, $A_L = 3.37$, and $A_S = 0.80$ into Eq. (2) allows to determine $k = 0.15$ for the U solubility coefficient. Consequently, weathering processes imply that uranium released into solution corresponds to 15% of that occurring in rocks. Such U-isotopes approach utilizing ^{238}U and ^{234}U as natural weathering indicators is advantageous compared to Na, Ca, Mg, and Fe as considered in this paper because (1) the U atmospheric inputs can be disregarded and (2) it is possible to estimate the fraction of U that solubilizes from the rock matrices. Because of these reasons, Moreira-Nordemann (1980,

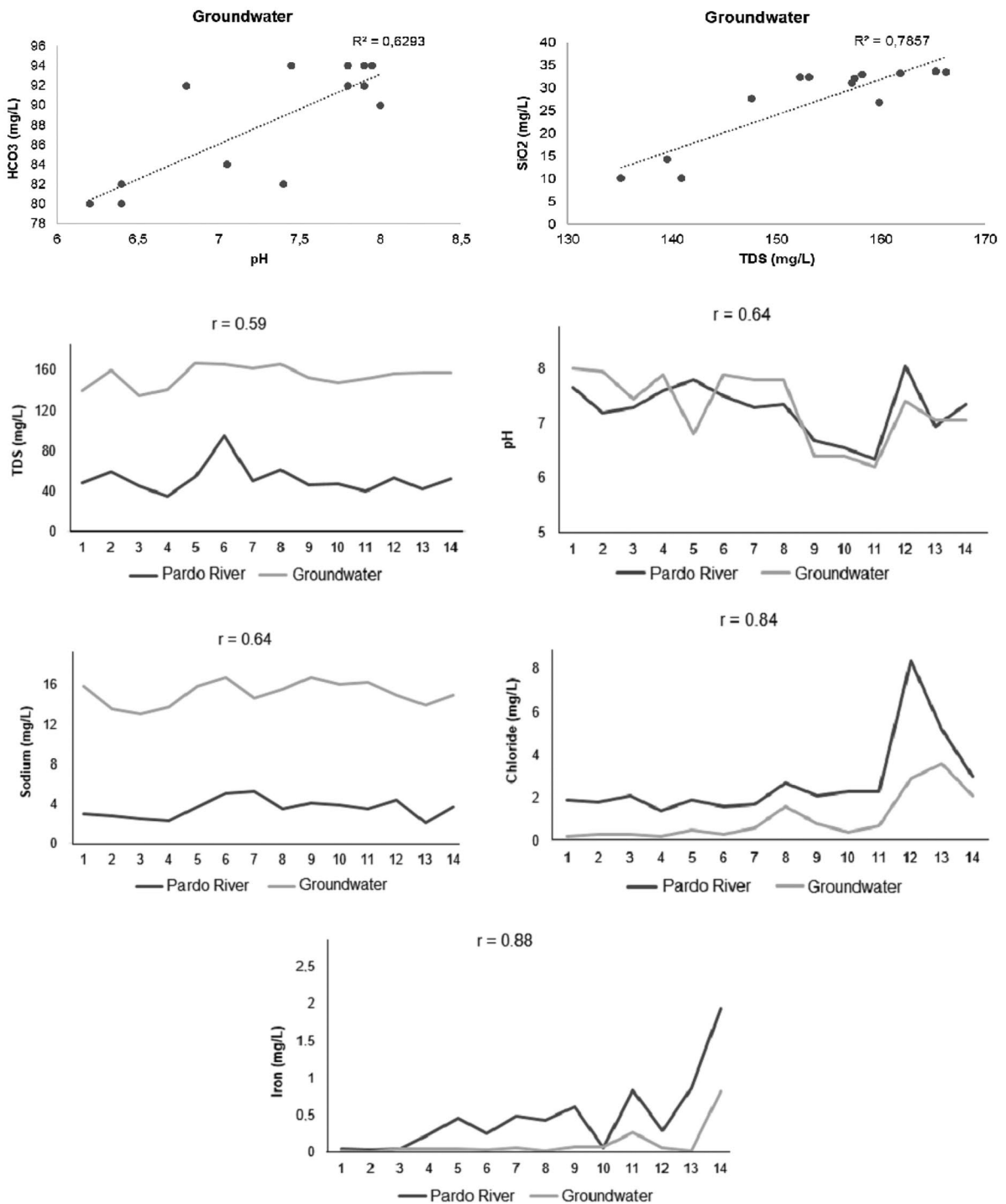
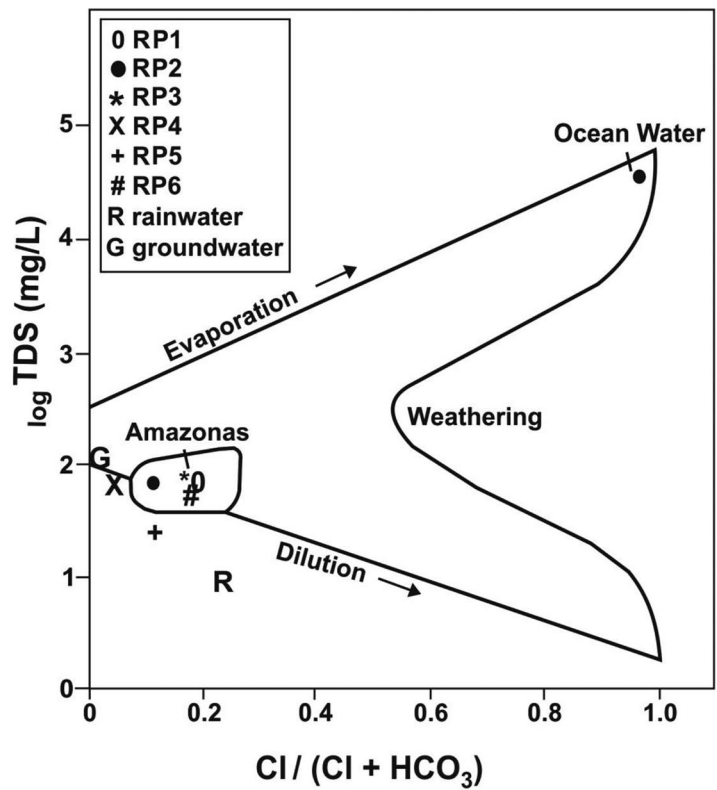
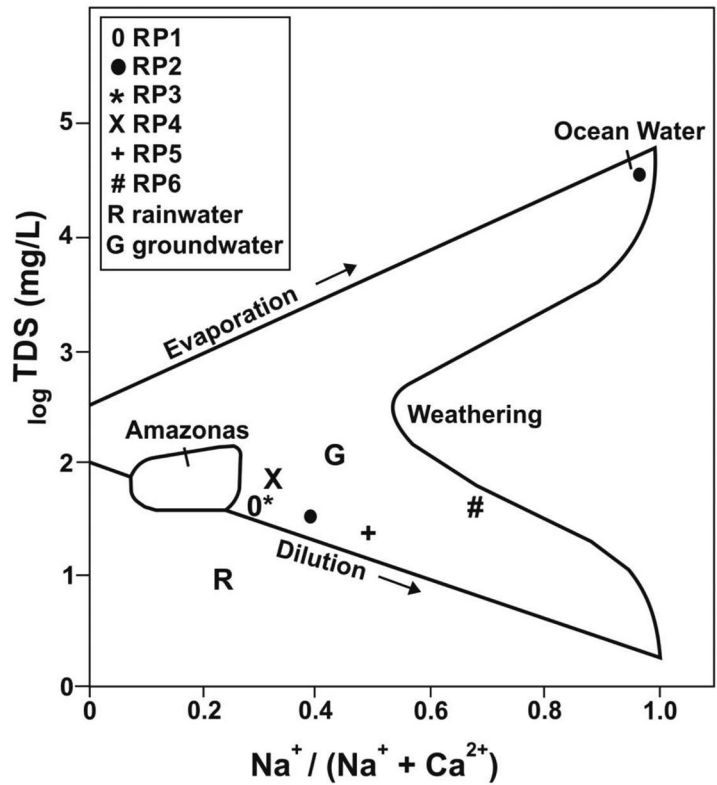


Fig. 9 (Top) Bicarbonate vs. pH and silica vs. TDS relationships for the groundwater samples exploiting the GAS and Serra Geral aquifers. (Remainder) Relationships for param-

eters measured during the sampling period of September 2017 to November 2018 for the groundwaters and surface waters of Pardo River

Fig. 10 Use of the Gibbs (1970) boomerang diagrams for plotting the data obtained in the analysis of the water samples. The codes of the samples are the same of those shown in Table 1



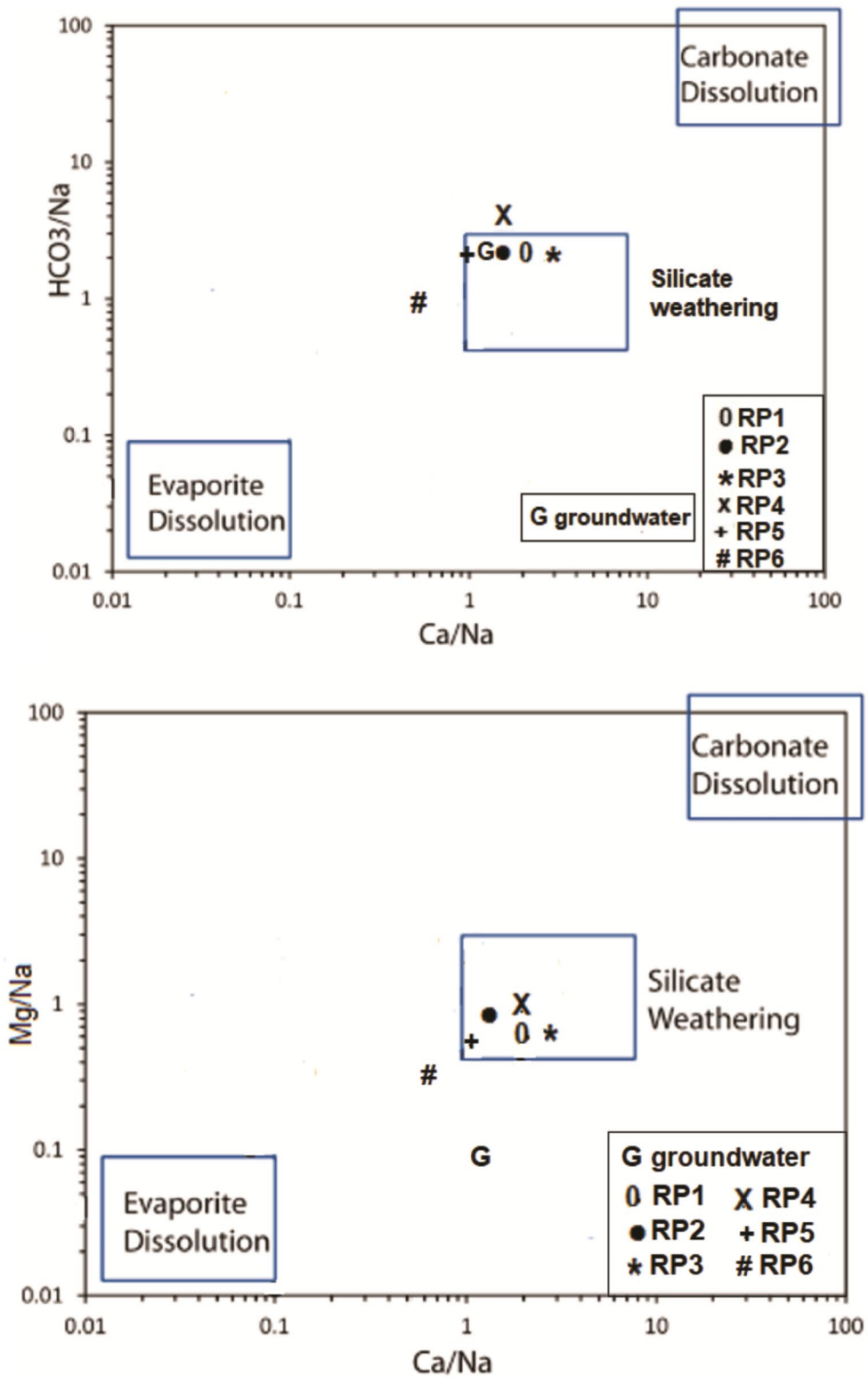


Fig. 11 Use of the $\text{HCO}_3^-/\text{Na}^+$ vs. $\text{Ca}^{2+}/\text{Na}^+$ and $\text{Mg}^{2+}/\text{Na}^+$ vs. $\text{Ca}^{2+}/\text{Na}^+$ graphs for plotting the results of the chemical analysis of the water samples from the study area

Table 4 Total flux, rainfall deposition, net flux, and chemical weathering rate in the Pardo River watershed, São Paulo State, Brazil

Parameter	Unit	Total flux	Rainfall deposition	Net flux	Weathering rate
Na ⁺	ton/km ² yr	0.58	0.52	0.06	11.43
K ⁺	ton/km ² yr	0.30	0.50	-0.20	nc
Ca ²⁺	ton/km ² yr	1.12	1.02	0.10	2.76
Mg ²⁺	ton/km ² yr	0.22	0.18	0.04	3.17
SiO ₂	ton/km ² yr	3.01	3.14	-0.13	nc
HCO ₃ ⁻	ton/km ² yr	4.07	6.14	-2.07	nc
Cl ⁻	ton/km ² yr	0.86	1.86	-1.00	nc
NO ₃ ⁻	ton/km ² yr	0.25	2.37	-2.12	nc
SO ₄ ²⁻	ton/km ² yr	0.26	0.87	-0.61	nc
Fe	ton/km ² yr	0.049	0.014	0.035	0.77
PO ₄ ³⁻	ton/km ² yr	0.013	nc	nc	nc
NO ₂ ⁻	(× 10 ⁻²) ton/km ² yr	0.13	0.68	-0.55	nc
Ba	(× 10 ⁻²) ton/km ² yr	0.020	0.79	-0.77	nc
Sr	(× 10 ⁻²) ton/km ² yr	1.02	0.60	0.42	nc
Ni	(× 10 ⁻²) ton/km ² yr	2.30	0.22	2.08	nc
Cu	(× 10 ⁻²) ton/km ² yr	0.18	0.42	-0.24	nc
Zn	(× 10 ⁻²) ton/km ² yr	0.98	0.69	0.29	nc
Mn	(× 10 ⁻²) ton/km ² yr	0.09	0.42	-0.33	nc
Cr	(× 10 ⁻²) ton/km ² yr	0.020	0.088	-0.068	nc
Pb	(× 10 ⁻²) ton/km ² yr	0.24	0.12	0.12	nc
U	(× 10 ⁻⁶) ton/km ² yr	1.93	see text	See text	See text

nc not calculated

1984) modified Eq. (1), including the dimensionless parameter (k) into the formula:

$$W = F_E/k \cdot E_R \quad (3)$$

Thus, considering this modified equation, the corrected chemical weathering rate is 8.64 t/km² year instead of 1.30 t/km² year that is a value almost 6.6 times higher. Uranium in the following Brazilian watersheds yielded higher chemical weathering rates than that obtained in this study: Preto River, Bahia State, 100 t/km² year (Moreira-Nordemann, 1980); Corumbataí River, São Paulo State, 41.2 t/km² year (Conceição & Bonotto, 2003); Upper Sorocaba River, São Paulo State, 36.6 t/km² year (Sardinha et al., 2010). Additionally, chemical weathering rates lower (0.093–5.16 t/km² year) and higher (18.48 and 19.84 t/km² year) than 8.64 t/km² year have been reported by Bonotto (2022a, b) utilizing U measured in seven water bodies of Araxá City, Minas Gerais State, Brazil.

The chemical weathering rate (W) in Eqs. (1) and (3), as well the rocks density (ρ) may be used to calculate the linear weathering rate in watersheds (v), based on the formula (Moreira-Nordemann, 1980, 1984):

$$v = W/\rho \quad (4)$$

The density of typical rocks of the PSB has been reported by Tratz and Silva (2009) and Cunha et al. (2016), for instance: between 2.8 and 3.0 g/cm³ for rocks of the Serra Geral Formation and 2.2 g/cm³ for rocks of the Bauru Group. Therefore, these values yield a mean density of 2.55 g/cm³ for the dominant rocks in the study area. Thus, for U, Eq. (4) allows estimating a linear weathering rate of 3.4 $\mu\text{m}/\text{year}$ (3.4 mm/ka), indicating that 1 m of rock disposed vertically requires about 294 ka to be altered, under the present climatic conditions. Uranium in the following Brazilian hydrographic basins permitted estimate linear weathering rates higher than 3.4 $\mu\text{m}/\text{year}$ as obtained in this study (Bonotto, 2022a; Conceição & Bonotto, 2003; Moreira-Nordemann, 1980, 1984; Sardinha et al., 2010): 37 $\mu\text{m}/\text{year}$, Preto River (Bahia State); 13.0 $\mu\text{m}/\text{year}$, Salgado River (Bahia State); 17.9 $\mu\text{m}/\text{year}$, Corumbataí River (São Paulo State); 14.1 $\mu\text{m}/\text{year}$, Upper Sorocaba River (São Paulo State); 6.2 and 6.6 $\mu\text{m}/\text{year}$, two water bodies from Araxá city (Minas Gerais State). However, the linear rate of 3.4 $\mu\text{m}/$

year is higher than the range of 0.031–1.72 $\mu\text{m}/\text{year}$ as reported in five water bodies of Araxá City, Minas Gerais State (Bonotto, 2022a).

Therefore, these chemical weathering rates calculations vary according to the choice of the element utilized. The utility of U has been confirmed for such purpose in the study area, and several factors may be attributed to explain the different values found in the hydrographic basins where this radioelement and its isotopes ^{238}U and ^{234}U have been used, for instance, temperature, rainfall, altitude, terrain slope, lithology, and distribution in the mineralogical assembly, among others.

Conclusions

This study focused Pardo River hydrographic basin located at Center/Southwest region of São Paulo State, Brazil. The major tools consisted on the use of hydrochemical and natural radionuclides (^{238}U , ^{234}U , and ^{210}Po) data. Surface water and groundwater samples were submitted to the same methods for measuring physicochemical parameters (pH, redox potential Eh, EC-electrical conductivity), silica, major dissolved cations (sodium, potassium, calcium, magnesium) and anions (bicarbonate, chloride, nitrate, sulfate), trace elements (Fe, Mn Cu, Zn, Ni, Ba, Sr, Pb, etc.), and natural radionuclides. Rainwater, surface waters, and groundwaters data were comparatively evaluated by hydrogeochemical diagrams, which highlighted that except for chloride and nitrate, all other major constituents are depleted in rainwater. pH and Eh correlated inversely in the groundwaters exploiting the Guarani Aquifer System and Serra Geral aquifer. Calcium is the cation slightly preponderant in the waters, while bicarbonate is the dominant anion as evidenced by the Piper and Schoeller diagrams. The Gibbs boomerang diagrams suggested that the chemical composition of the surface waters and groundwaters is chiefly controlled by the amount of dissolved salts supplied by precipitation, but plots of the ratios HCO_3/Na vs. Ca/Na and Mg/Na vs. Ca/Na plots pointed out how important are the effects of weathering of silicates on their composition. Low saline and sodic waters have been evidenced by the sodium adsorption ratio (SAR) vs. EC diagram, suggesting their possible use for irrigation and growing plants in agricultural soils.

Surface water-groundwater interactions have been evidenced by significant correlations found for the parameters pH, TDS (total dissolved solids), Na, Cl, and Fe as measured in samples collected from September 2017 to November 2018. When the net flux in the Pardo River exutory was positive (total discharge flux higher than the input flux due to wet deposition), the chemical data obtained by X-ray fluorescence for typical rocks occurring in the basin allowed to estimate weathering rates. This was the case for sodium, calcium, magnesium, and iron that provided chemical weathering rates ranging from 0.77 (Fe) to 11.43 $\text{t}/\text{km}^2 \text{ year}$ (Na). The U-atmospheric correction was not necessary as its concentration in rainwater is lower than 0.002 $\mu\text{g}/\text{L}$, implying on a flux value of $1.93 \times 10^{-6} \text{ t}/\text{km}^2 \text{ year}$ at the Pardo River exutory. Thus, an initial weathering rate of 1.30 $\text{t}/\text{km}^2 \text{ year}$ was determined considering the U presence in the basin and afterwards corrected to 8.64 $\text{t}/\text{km}^2 \text{ year}$ taking into account the U-dissolution coefficient of 0.15 as determined from measurements of the natural uranium isotopes ^{238}U and ^{234}U in samples of rocks, soils, and waters occurring at the study area. From the value of 8.64 $\text{ton}/\text{km}^2 \text{ year}$, it has been possible to estimate a linear weathering rate of 3.4 $\mu\text{m}/\text{year}$ (3.4 mm/ka), suggesting that $\sim 294 \text{ ka}$ is needed to the alteration of 1 m of rock, under the present climatic conditions. The literature reports equivalent values of rates, which vary depending on factors like temperature, rainfall, altitude, terrain slope, lithology, and elements distribution in the mineralogical assembly, among others.

Acknowledgements Prof. Upmalu Lall, Columbia University, New York, is grateful for the support given in order to write this paper. One anonymous reviewer is greatly thanked for helpful comments that improved the readability of this manuscript.

Author contribution Not applicable.

Funding This study was funded by the Brazilian agencies CNPq-National Council for Scientific and Technological Development (Grant 304010/2021–9) and FAPESP-Foundation for Supporting Research at São Paulo State (Grants 2014/50945–4 and 2021/11737–0).

Availability of data The author declares that all available data are reported in this paper.

Code availability Not applicable.

Declarations

Ethical statement This is an observational study that did not involve human participants or biological materials, thus, not requiring ethical approval of the Research Ethics Committee of the authors' institution.

Ethical responsibilities of author The author has read, understood, and has complied as applicable with the statement on "Ethical responsibilities of Authors" as found in the Instructions for Authors.

Consent to participate The author DMB gives explicit consent to participate in the publication of this manuscript into *Environmental Monitoring and Assessment*.

Consent for publication The author DMB agreed with the content of the manuscript, giving explicit consent to its submission for publication into *Environmental Monitoring and Assessment*.

Conflict of interest The author declares no competing interests.

References

- Albarelli, D. S. N. A. (2013). *Depositional environments and ceramic characterization of Araçatuba Formation (Bauru basin) at Santo Anastácio River valley, São Paulo State*. Monograph. Campinas: UNICAMP-University of Campinas. (in Portuguese).
- Anjinho, P., Barbosa, M., Costa, C. W., & Mauad, F. F. (2020). Environmental fragility analysis in reservoir drainage basin land use planning: A Brazilian basin case study. *Land Use Policy*, 100. <https://doi.org/10.1016/j.landusepol.2020.104946>
- Baas Becking, L. G. M., Kaplan, I. R., & Moore, D. (1960). Limits of the natural environment in terms of pH and oxidation-reduction potential. *Journal of Geology*, 68, 243–284.
- Baskaran, M. (1995). A search for the seasonal variability on the depositional fluxes of ^7Be and ^{210}Pb . *Journal of Geophysical Research*, 100, 2833–2840.
- Baskaran, M. (2012). *Handbook of Environmental Isotope Geochemistry*. Berlin: Springer.
- Bertin, L. (1974). *The new Larousse Encyclopedia of the Earth*. New York: Crown Publishers Inc.
- Birke, M., Rauch, U., Lorenz, H., & Kringel, R. (2010). Distribution of uranium in German bottled and tap water. *Journal of Geochemical Exploration*, 107, 272–282.
- Bonotto, D. M. (2006). Hydro(radio)chemical relationships in the giant Guarani aquifer, Brazil. *Journal of Hydrology*, 323, 353–386.
- Bonotto, D. M. (2010). *The Poços de Caldas Hot Spot: A big blast for nuclear energy in Brazil*. New York: Nova Science.
- Bonotto, D. M. (2017). The dissolved uranium concentration and $^{234}\text{U}/^{238}\text{U}$ activity ratio in groundwaters from spas of southeastern Brazil. *Journal of Environmental Radioactivity*, 166, 142–151.
- Bonotto, D. M. (2022a). U-isotopes and weathering rates in watersheds of Araxá city, Minas Gerais State, Brazil. *Journal of Environmental Radioactivity*, 246, 106835.
- Bonotto, D. M. (2022b). Hydrochemical and radiometric evaluation of fresh and thermal waters from Araxá city (Minas Gerais, Brazil). *Environmental Geochemistry and Health*, 44, 2163–2186.
- Bonotto, D. M., Caprioglio, L., Bueno, T. O., & Lazarindo, J. R. (2009). Dissolved ^{210}Po and ^{210}Pb in Guarani aquifer groundwater, Brazil. *Radiation Measurements*, 44, 311–324.
- Bonotto, D. M., Jiménez-Rueda, J. R., Fagundes, I. C., & Fonseca Filho, C. R. A. (2017). Weathering processes and dating of soil profiles from São Paulo State, Brazil, by U-isotopes disequilibria. *Applied Radiation and Isotopes*, 119, 6–15.
- Bonotto, D. M., & Roveratti, G. (2017). Hydrochemical analysis of groundwater from Brazilian aquifers by TXRF analysis. In H. Bailey (Ed.), *Aquifers: Properties, roles and research* (pp. 57–79). New York: Nova Science.
- Bonotto, D. M., & Roveratti, G. (2020). Comparative geochemical analysis by XRF of sediments for limnological studies. In B. Veress & J. Szigethy (Eds.), *Horizons in Earth Science Research* (Vol. 20, pp. 41–64). New York: Nova Science.
- Bonotto, D. M., & Silveira, E. G. (2003). Preference ratios for mercury and other chemical elements in the Madeira river, Brazil. *Journal of South American Earth Sciences*, 15, 911–923.
- Bonotto, D. M., & Thomazini, F. O. (2019). Comparative study of mineral and surface waters of Araxá spa, Minas Gerais State, Brazil. *Environmental Earth Sciences*, 78, 542.
- Brasil. (1997). *Federal Law 9433 of 8th January 1997. Establishes the national water resources policy and creates the national water resources management system*. Presidency of Republic: Brasília. (in Portuguese).
- Brownlow, A. H. (1996). *Geochemistry*. Prentice Hall: Upper Saddle River.
- Capobianco, J. P. R., & Whately, M. (2002). *Billings 2000: Threats and prospects for the largest water reservoir in the metropolitan region of São Paulo. Report on the participatory socio-environmental diagnosis of the Billings watershed in the period 1989–1999*. Instituto Socioambiental: São Paulo. (in Portuguese).
- Cavalchuki, L. C. (2021). *History of Pardo River*. Retrieved December 1, 2021, from <http://riopardovivo.org/historico-do-rio-pardo/>. (in Portuguese).
- CBH-MP (Comitee of Medium Paranapanema hydrographic basin). (1999). *Basin plan of the Medium Paranapanema water resources management unit*. CBH-MP: Marília. (in Portuguese).
- CBH-MP (Comitee of Medium Paranapanema hydrographic basin). (2019). *Report of the hydric resources situation*. CBH-MP: Marília. (in Portuguese).
- CBH-RP (Comitee of the Paranapanema River hydrographic basin). (2016). *Executive report of the integrated plan of hydric resources from the Management Unit of Paranapanema Hydric Resources*. CBH-RP: Marília. (in Portuguese).
- Chabaux, F., Riotte, J., Clauer, N., & France-Lanord, C. (2001). Isotopic tracing of the dissolved U fluxes of Himalayan rivers: Implications for present and past U budgets of the Ganges-Brahmaputra system. *Geochimica Et Cosmochimica Acta*, 65(19), 3201–3217.

- Chabaux, F., Dequincey, O., Lévêque, J.-J., Leprun, J.-C., Clauer, N., Riotte, J., & Paquet, H. (2003). Tracing and dating recent chemical transfers in weathering profiles by trace-element geochemistry and ^{238}U - ^{234}U - ^{230}Th disequilibria: The example of the Kaya lateritic toposequence (Burkina-Faso). *CR Geoscience*, *335*, 1219–1231.
- Coelho Netto, A. L. (2005). Slope hydrology at the interface with geomorphology. In A. J. T. Guerra, & S. B. Cunha (Eds.), *Geomorphology: An update of bases and concepts*, (6th ed., pp. 93–148). Ed. Bertrand Brasil: Rio de Janeiro. (in Portuguese).
- Conceição, F. T., & Bonotto, D. M. (2003). Use of U-isotope disequilibrium to evaluate the weathering rate and fertilizer-derived uranium in São Paulo State, Brazil. *Environmental Geology*, *44*, 408–418.
- Cresswell, R. G., & Bonotto, D. M. (2008). Some evolutionary scenarios by ^{36}Cl measurements in Guarani aquifer groundwaters. *Applied Radiation and Isotopes*, *66*, 1160–1174.
- Cunha, A. S., Adriano, L. B., Perosi, F. A., Cabrera, M. H. G., Adriano, M. S., Terra, E. F., Fontes, S. L., & Silva, D. S. (2016). Gravity imaging at Northern Paraná basin: Airborne gravity data analysis and forward modeling simulations. *Brazilian Journal of Geophysics*, *34*(4), 479–494.
- DAEE (Department of Waters and Electric Energy). (2021). *Rainfall and flow rate at Pardo River basin*. Retrieved December 1, 2021, from <http://www.daee.sp.gov.br/site/acervo/>. (in Portuguese).
- Dellinger, M., Bouchez, J., Gaillardet, J., Faure, L., & Moureau, J. (2017). Tracing weathering regimes using the lithium isotope composition of detrital sediments. *Geology*, *45*(5), G38671.1.
- Dibogo, E. P. (2007). *Environmental planning of the Cedro stream hydrographic basin*. MSc Dissertation. Presidente Prudente: UNESP-São Paulo State University. (in Portuguese).
- Dosseto, A., Bourdon, B., & Turner, S. P. (2008). Uranium-series isotopes in river minerals: Insights into the time-scales of erosion and sediment transport. *Earth and Planetary Science Letters*, *265*, 1–17.
- Duan, L., Hao, J., Xie, S., Zhou, Z., & Ye, X. (2002). Determining weathering rates of soils in China. *Geoderma*, *110*(3–4), 205–225.
- EarthLabs. (2022). *Lab 1: Think globally, act locally*. Retrieved December 1, 2021 from <https://serc.carleton.edu/eslabs/climate/1a.html>
- Fernandes, L. A. (2004). Lithostratigraphic map of the eastern part of the Bauru basin (PR, SP, MG), scale 1:1,000,000. *Paraná Geosciences Bulletin*, *55*, 53–66. (in Portuguese).
- Fernandes, A. M., Conceição, F. T., Spatti, E. P., Jr., Sardinha, D. S., & Mortatti, J. (2016). Chemical weathering rates and atmospheric/soil CO_2 consumption of igneous and metamorphic rocks under tropical climate in southeastern Brazil. *Chemical Geology*, *443*, 54–66.
- Flynn, W. W. (1968). The determination of low levels of Polonium-210 in environmental materials. *Analytica Chimica Acta*, *43*, 221–227.
- Freitas, E. V. S., Nascimento, C. W. A., Goulart, D. F., & Silva, J. P. S. (2009). Cadmium and lead availability to corn in soil amended with phosphorus fertilizers. *Brazilian Review of Soil Science*, *33*(6), 1899–1907. (in Portuguese).
- Fritz, P., & Fontes, J. C. (1980). *Handbook of Environmental Isotope Geochemistry*. Amsterdam: Elsevier.
- Gaillardet, J., Dupré, P., Louvat, P., & Allègre, C. J. (1999). Global silicate weathering and CO_2 consumption rates deduced from the chemistry of large rivers. *Chemical Geology*, *159*, 3–30.
- Garrels, R. M., & MacKenzie, F. T. (1967). Origin of the chemical compositions of some springs and lakes. In ACS-American Chemical Society (Ed.), *Equilibrium concepts in natural water systems* (Advances in Chemistry Series, v. 67, pp. 222–242). Washington: ACS.
- Gibbs, R. J. (1970). Mechanisms controlling world water chemistry. *Science*, *170*, 1088–1090.
- Grasby, S. E., & Hutcheon, I. (2000). Chemical dynamics and weathering rates of a carbonate basin, Bow River, southern Alberta. *Applied Geochemistry*, *15*, 66–77.
- Hach. (2000). *Water Analysis Handbook* (4th ed.). Hach Co: Loveland.
- IBGE (Brazilian Institute of Geography and Statistics). (2002). *Brazil weather map*. IBGE. (in Portuguese).
- IPT (Technological Researches Institute of São Paulo State). (1981). *Geomorphological map of São Paulo State: 1:1,000,000*, v 2. São Paulo: IPT. (in Portuguese).
- Ivanovich, M., & Harmon, R. S. (1992). *Uranium Series Disequilibrium: Applications to Environmental Problems*. Clarendon Press.
- Jeter, H. W. (2000). Determining the ages of recent sediments using measurements of trace radioactivity. *Terra Et Aqua*, *78*, 21–28.
- Krauskopf, K. B., & Bird, D. K. (1995). *Introduction to geochemistry*. New York: McGraw-Hill Inc.
- Krishnaswami, S., Williams, G. A., Graustein, W. C., & Turekian, K. K. (2004). The effect of weathering regime on uranium decay series and osmium in two soil profiles. *Geochemical Journal*, *38*, 651–660.
- Kumar, P. J. S. (2014). Evolution of groundwater chemistry in and around Vaniyambadi industrial area: Differentiating the natural and anthropogenic sources of contamination. *Chemistry of the Earth*, *74*, 641–651.
- Laporte, L. F. (1969). *Ancient sedimentation (environments)*. São Paulo. (in Portuguese).
- Leal, A. C. (1995). *Environment and urbanization in the microbasin of Areia Branca – Campinas (SP)*. MSc Dissertation. Rio Claro: UNESP-São Paulo State University. (in Portuguese).
- Lima, W. P. (2006). *Introduction to the management of hydrographic basins*. DCFL/ESALQ/USP – São Paulo University: Piracicaba. (in Portuguese).
- Milani, E. J., Melo, J. H. G., Souza, P. A., Fernandes, L. A., & França, A. B. (2007). Paraná basin. *Geosciences Bulletin of Petrobras*, *15*(2), 265–287. (in Portuguese).
- Milani, E. J., & Ramos, V. A. (1998). Paleozoic orogenies in the south-western domain of Gondwana and subsidence cycles of Paraná basin. *Brazilian Journal of Geology*, *28*(4), 473–484. (in Portuguese).
- Millot, R., Gaillardet, J., Dupré, B., & Allègre, C. J. (2002). The global control of silicate weathering rates and the coupling with physical erosion: New insights from rivers of the Canadian Shield. *Earth and Planetary Science Letters*, *96*, 83–98.
- Mirabbasi, R., Mazloumzadeh, S. M., & Rahnama, M. B. (2008). Evaluation of irrigation water quality using Fuzzy Logic. *Research Journal of Environmental Sciences*, *2*, 340–352.

- Moreira-Nordemann, L. M. (1980). Use of $^{234}\text{U}/^{238}\text{U}$ disequilibrium in measuring chemical weathering rate of rocks. *Geochimica Et Cosmochimica Acta*, 44, 103–108.
- Moreira-Nordemann, L. M. (1984). Salinity and weathering rate of rocks in a semi-arid region. *Journal of Hydrology*, 71, 131–147.
- Morelato, R. (2017). *Paraná basin: Geological summary and sectors on offer*. ANP-Brazilian Petroleum Agency: Brasília. (in Portuguese).
- Netto, A. S. T. (1980). *Sedimentology manual*. Petrobras/SEPEs/DIVEN: Salvador. (in Portuguese).
- Oliveira, J. B., Camargo, M. N., Rossi, M., & Calderano Filho, B. (1999). *Pedological map of São Paulo State – Expanded legend*. Instituto Agrônômico/EMBRAPA Solos: Campinas. (in Portuguese).
- Osmond, J. K., & Cowart, J. B. (1976). The theory and uses of natural uranium isotopic variations in hydrology. *Atomic Energy Review*, 14, 621–679.
- Ouma, K. O., Shane, A., & Syampungani, S. (2022). Aquatic ecological risk of heavy-metal pollution associated with degraded mining landscapes of the Southern Africa river basins: A review. *Minerals*, 12, 225.
- Paços, T. (1983). Rate constants of dissolution derived from the measurement of mass balance in hydrologic catchments. *Geochimica Et Cosmochimica Acta*, 47, 1855–1863.
- Perrotta, M. M., Salvador, E. D., Lopes, R. C., D'Agostino, L. Z., Peruffo, N., Gomes, S. D., Sachs, L. L. B., Meira, V. T., Garcia, M. G. M., & Lacerda Filho, J. V. (2005). *Geological map of São Paulo State – Scale 1:750,000*. CPRM (Brazilian Geological Survey): São Paulo. (in Portuguese).
- Piper, A. M. A. (1944). A graphic procedure in the geochemical interpretation of water-analyses. *Transactions of the American Geophysical Union*, 25, 914–928.
- Pirolí, E. L. (2013). *Geoprocessing applied to the land study of permanent preservation areas in water bodies from Pardo River hydrographic basin*. Post PhD Thesis. Ourinhos: UNESP-São Paulo State University. (in Portuguese).
- Riebe, C. S., Kirchner, J. W., & Finkel, R. C. (2003). Long-term rates of chemical weathering and physical erosion from cosmogenic nuclides and geochemical mass balance. *Geochimica Et Cosmochimica Acta*, 67(22), 4411–4427.
- Rodrigues, C., & Adami, S. (2005). Fundamental techniques applied to the study of hydrographic basins. In L. A. B. Venturi (Ed.), *Practicing Geography: Field and laboratory techniques* (pp. 147–166). Oficina de Textos: São Paulo. (in Portuguese).
- Ross, J. L. S., & Moroz, I. C. (1997). *Geomorphological map of São Paulo State*. DGFFLCH-USP, IPT, FAPESP: São Paulo. (in Portuguese).
- Safre, A. L. S., & Manzione, R. L. (2015). Precipitation estimate at Pardo River basin in the summer of 2013/2014 and effects on the municipalities of UGRHI-17. In *Proc. XVI Brazilian of Remote Sensing* (pp. 4868–4874). João Pessoa. (in Portuguese).
- Sardinha, D. S., Bonotto, D. M., & Conceição, F. T. (2010). Weathering rates at Alto Sorocaba basin, Brazil, using U-isotopes and major cations. *Environmental Earth Sciences*, 61, 1025–1036.
- Schoeller, H. (1962). *Groundwaters*. Masson & Cie: Paris. (in French).
- Schulz, M. S., & White, A. F. (1999). Chemical weathering in tropical watershed, Luquillo mountains, Puerto Rico III: Quartz dissolution rate. *Geochimica Et Cosmochimica Acta*, 63, 337–350.
- SIAGAS (Information system of groundwaters). (2022). *General data of well 3500007447*. Retrieved December 1, 2021, from <http://siagasweb.cprm.gov.br/layout/detalhe.php?ponto=3500007447>. (in Portuguese).
- Silva, R. B. G. (1983). *Hydrochemical and isotopic study of groundwaters from Botucatu aquífer at São Paulo State*. PhD Thesis. São Paulo: USP-São Paulo University. (in Portuguese).
- Silva, A. J. P., Lopes, R. C., Vasconcelos, A. M., Bahia, R. B. C. (2003). Inner Paleozoic and Meso-Cenozoic sedimentary basins. In L. A. Bizzi, C. Schobbenhaus, R. M. Vidotti, & J. H. Gonçalves (Eds.), *Geology, Tectonics and Mineral Resources of Brazil* (v. 581, pp. 55–85). CPRM (Brazilian Geological Survey): Brasília. (in Portuguese).
- Small, E. F., Anderson, R. S., & Hancock, G. S. (1999). Estimates of the rate of regolith production using ^{10}Be and ^{26}Al from an alpine hillslope. *Geomorphology*, 27, 131–150.
- Soler i Gil, A., & Bonotto, D. M. (2015). Hydrochemical and stable isotopes (H, O, S) signatures in deep groundwaters of Paraná basin, Brazil. *Environmental Earth Sciences*, 73, 95–113.
- Sracek, O., & Hirata, R. (2002). Geochemical and stable isotopic evolution of the Guarani Aquifer System in the state of São Paulo, Brazil. *Hydrogeology Journal*, 10, 643–655.
- Tratz, E. B., & Silva, P. A. H. (2009). Analysis of volcanic rocks from Paraná basin based on the relief characteristics and landscape differences using petrographic analysis and interpretation of the Digital Terrain Model (DTM) at Guarapuava municipality, Paraná, Brazil. In *Proc. XII EGAL – Latin America Geographers Meeting* (pp. 1–10). Montevideo. (in Portuguese).
- USSL (US Salinity Laboratory Staff). (1954). *Diagnosis and improvement of saline and alkali soils*. Handbook No. 60, US Department of Agriculture.
- van der Aa, M. (2003). Classification of mineral water types and comparison with drinking water standards. *Environmental Geology*, 44, 554–563.
- van de Wiel, H. J. (2003). *Determination of elements by ICP-AES and ICP-MS*. Bilthoven, The Netherlands: National Institute of Public Health and the Environment (RIVM).
- Waterloo Hydrogeologic. (2003). *AquaChem User's manual: Water quality data analysis, Plotting & modeling*. Waterloo Hydrogeologic: Waterloo.
- White, A. F., & Blum, A. E. (1995). Effects of climate on chemical weathering in watersheds. *Geochimica Et Cosmochimica Acta*, 59, 1729–1747.
- WHO (World Health Organization). (2011). *Guidelines for drinking water quality*. WHO Press: Geneva.
- Wilcox, L. V. (1955). *Classification and use of irrigation waters*. USDA Circular No. 969, U.S. Department of Agriculture.
- Young, H. D. (1962). *Statistical treatment of experimental data*. New York: McGraw Hill.

Publisher's Note Springer Nature remains neutral with regard to jurisdictional claims in published maps and institutional affiliations.

Springer Nature or its licensor (e.g. a society or other partner) holds exclusive rights to this article under a publishing agreement with the author(s) or other rightsholder(s); author self-archiving of the accepted manuscript version of this article is solely governed by the terms of such publishing agreement and applicable law.